Computational Biology and Chemistry 120 (2026) 108724

Contents lists available at ScienceDirect

Computational Biology and Chemistry

journal homepage: www.elsevier.com/locate/cbac

Stability and dynamics of fractional order frogeye leaf spot infection model with fungal density function

Muhammad Farman [a,b,c,*], Izhar Ullah [a], Evren Hincal [a,d], Kottakkaran Sooppy Nisar [e,f], Kamyar Hosseini [a,d,g], Aceng Sambas [b,h]

[a] Faculty of Arts and Sciences, Department of Mathematics, Near East University, Nicosia 99010, Cyprus
[b] Faculty of Informatics and Computing, Universiti Sultan Zainal Abidin, Besut Campus, Terengganu 22200, Malaysia
[c] Jadara University Research Center, Jadara University, Irbid, Jordan
[d] Research Center of Applied Mathematics, Khazar University, Baku, Azerbaijan
[e] Department of Mathematics, College of Science and Humanities in Al-Kharj, Prince Sattam bin Abdulaziz University, 11942 Al-Kharj, Saudi Arabia
[f] Department of Mathematical Sciences, Saveetha School of Engineering, SIMATS, Chennai, 602105, Tamilnadu, India.
[g] Faculty of Engineering and Natural Sciences, Istanbul Okan University, Istanbul, Turkey
[h] Department of Mechanical Engineering, Universitas Muhammadiyah Tasikmalaya, Tasikmalaya 46196, Indonesia

ARTICLE INFO

Keywords:
Mathematical model
Plant disease
Caputo derivative
Stability
Approximate solution

ABSTRACT

This article presents a fractional-order model for frog eye leaf spot in soybean plants using the Caputo fractional derivative. The study validates the model, estimates solutions using reliable numerical algorithms. Comparing numerical simulations to earlier integer-order models demonstrates how well fractional calculus captures the intricacy of disease dynamics. The research aims to enhance soybean crop health and yield through improved disease control strategies and mathematical modeling of plant pathology. Using fractional calculus, the model is analyzed to determine its boundedness, positivity, and unique solutions. The existence and uniqueness of the exact solution are further validated using fixed-point theory and the Lipschitz condition. Lyapunov functions are employed to verify the global stability of both the disease-free and endemic equilibrium points. The study explores the influence of the Caputo operator by solving the generalized power law kernel using a two-step Lagrange polynomial method. Fractional-order model outperforms integer-order models by accounting for biological memory effects and past disease history. It produces more accurate simulations that fit better with real-world data, improving their performance. The model's adaptability allows it to predict outbreaks and evaluate treatment strategies like crop rotation, fungicide use, and genetic resistance. It can also be used to treat other plant diseases. The model aids researchers in analyzing climate change's impact on disease transmission, promoting sustainable farming and food security, benefiting farmers, the agricultural sector, and the environment.

1. Introduction

Cercospora sojina, the causative agent of soybean frog-eye leaf spot, is typically found in warm, humid environments. Although the disease was first documented in the Midwest in the 1920s, no outbreaks have occurred in Iowa. In mid-July, the disease was visible and uniformly distributed across a 12-hectare no-till field planted with the cultivar Asgrow 2501. By the end of August, the disease had spread across more than 70 % of this field. However, in three nearby soybean fields, the disease incidence was less than ten percent. All 80 soybean varieties tested positive for the disease in central Iowa, where it was common in 1999 and 2000. C. sojina was discovered to have alkaline, straight, and multistage conidia. Warm winters in Iowa, a major soybean-producing state, caused outbreaks of frog-eye leaf spot, necessitating monitoring and surveys because they spread C. sojina seeds (Yang and Wang, 2023). It was discovered in several Iowa regions in 2000, with outbreaks in the soybean fields of Ames and Grand Junction in 1999. Four types of the disease had a severity of at least 40 % and were common in central Iowa. In Iowa, a significant seed-producing state in the northern soybean region, the disease needs to be monitored and surveyed because it is associated with warm winters (Athow and Probst, 1952). Cercospora sojina K. Hara, the disease that causes frog eye leaf spot (FLS), poses a serious threat to global soybean cultivation. This chapter investigates the various aspects of FLS, such as epidemiology, disease cycle,

* Corresponding author at: Faculty of Arts and Sciences, Department of Mathematics, Near East University, Nicosia 99010, Cyprus.
E-mail address: farmanlink@gmail.com (M. Farman).

https://doi.org/10.1016/j.compbiolchem.2025.108724
Received 20 June 2025; Received in revised form 16 September 2025; Accepted 8 October 2025
Available online 10 October 2025

pathogen biology, symptomatology, and management strategies. The disease's significance is demonstrated by its impact on soybean yield and quality. FLS-induced losses are primarily caused by a decrease in photosynthetic ability, early seed infection, defoliation, and inadequate pod formation. Depending on the favorable circumstances, yield losses have been reported to range from 10 % to 60 %, aggravating regional and global repercussions (Akem and Dashiell, 1994). An increasingly important method for improving observational and experimental research on biological phenomena is mathematical modeling. In order to understand plant virus disease epidemics, numerous mathematical models have been created utilizing a variety of methods and applications (see Murwayi et al., 2017; Blyuss et al., 2020; El Jarroudi et al., 2020; Agrawal et al., 2004; Zhao and Xiao, 2015; Amelia et al., 2021; Vyska et al., 2016).

The Fractional Calculus (FC), a variant of classical calculus, addresses integration and differentiation operations of non-integer order. It has turned out to be a useful mathematical tool in a number of academic disciplines, including biology, physics, engineering, and economics (see Nisar et al., 2024; Xu et al., 2025; Farman, Nisar, et al., 2025; Ullah et al., 2025; Farman et al., 2023, 2024; Farman, Sarwar, et al., 2025; Jiang et al., 2025; Narayanan et al., 2025; Ahmad et al., 2025). Frogeye leaf spot is a disease that can be effectively modeled using fractional calculus due to its polycyclic nature, which involves repeated cycles of infection, symptom development, and spore production. This results in complex, self-similar patterns at different scales, which fractional calculus can better capture than traditional integer-order models. Recent work, such as a mathematical model (Yang and Wang, 2023) for frogeye leaf spot epidemics using differential equations, highlights the ongoing relevance of this approach in understanding pathogen dynamics and predicting disease spread. The study in McDonald et al. (2022) developed an automated pipeline for measuring frogeye leaf spot lesions on soybean leaves, combining biological observation with computational analysis to generate high-resolution data for mathematical models. Another study (Phillips et al., 2021) using remote sensing analyzed the effect of foliar fungicides on frogeye leaf spot severity, revealing a correlation between disease severity and green leaf area and biomass. The study underscores the need for more comprehensive parameters and fractional approaches. A fractional-order 2-stage infection model is introduced in Ali et al. (2024) for plant diseases. In another model (Sharma et al., 2022), stated below, researchers divided the plant population into five subpopulations: Latent E_p, Protected B_p, Infected I_p, Post Infectious or Removed R_p, and Susceptible S_p. A fractional-order amendment of a BXW disease model, along with a few control measures, is defined in Manickam et al. (2024). The banana population N_p and the insect vector population N_v are the two population sizes included in the model. Researchers in El-Sayed et al. (2020) presented a fractional-order model of disease transmission for a two-stage infection, wherein exposed plants can also spread diseases, and a susceptible individual undergoes an exposed phase before becoming infectious. Some other works on fractional-order plant disease modeling are given in Nisar et al. (2024), Abdullah et al. (2024), Kumar et al. (2022), Ali et al. (2024), Ahmad et al. (2024), Ackora-Prah et al. (2023).

The study aims to develop and assess a mathematical model using the Caputo fractional operator to accurately depict the stability and dynamic behavior of frogeye leaf spot infections. The study utilizes fractional calculus, specifically Caputo fractional derivative, to enhance the understanding of memory and genetic aspects of disease transmission. The remaining portion of the paper is structured as follows. In Section 2, we develop our model and provide the necessary fractional calculus results. The key analysis of the model is given in Section 3 study of the model, which includes the positivity, boundness, and uniqueness of the solution. The qualitative analysis of the model, which includes the stability of equilibrium points, uniqueness, fundamental reproductive number, and sensitivity of parameters covered in Section 4. Stability of equilibrium points and chaos control of the system are discussed in Sections 5 and 6, respectively. In Section 7, the numerical scheme is shown. The consequences of the fractional order on the dynamics are also examined in Section 8, where numerical simulations support the derived theoretical results. Section 9 covers the concluding remarks and further suggestions.

2. Model formulation

Yang and Wang (2023) introduced a new differential equation-based mathematical model to investigate the transmission and spread of frog-eye leaf spot. The model considers the primary and secondary routes of disease transmission in addition to the intrinsic dynamics of the pathogen in the contaminated soil. Let's consider the following when calculating the number of plants per unit area in a field:

- $S(t)$: Susceptible (healthy) plants;
- $E(t)$: Plants exposed to infection;
- $I(t)$: Infected plants; and
- $R(t)$: Removed (post-infectious) plants.

Furthermore, let B stand for the Cercospora sojina fungal density of the soil. In this case, the total plant density in a field, which is taken to be constant, is

$$N = S + E + I + R.$$

Five state variables are represented by non-linear, coupled differential equations in the soybean model. The authors (Yang and Wang, 2023) proposed the following model to explain how frog-eye leaf spot soybean spreads and is transmitted in soybean plants:

$$\begin{aligned}
\frac{dS}{dt} &= \mu N - (\alpha I + \beta B)S - \mu S,\\
\frac{dE}{dt} &= \quad (\alpha I + \beta B)S - \mu E - \lambda E,\\
\frac{dI}{dt} &= \lambda E - \mu I - \delta I,\\
\frac{dR}{dt} &= \delta I - \mu R,\\
\frac{dB}{dt} &= rB\left(1 - \frac{B}{k}\right) - \tau B + \xi I.
\end{aligned} \tag{1}$$

The susceptible (healthy) plants grow naturally at the rate of μ. They acquire infection either by primary inoculum (β) from soil fungus or secondary inoculum (α) from infected plants. They then proceed into the exposed and infected compartment. Based on the law of mass action, a bilinear incidence is used to represent the two modes of transmission. The incidence rate is directly proportional to the product of the densities of susceptible and infectious plants. At a rate of $\frac{1}{\lambda}$, exposed plants go through a latent phase before spreading the disease and entering the infectious compartment. μ is also used to represent the natural removal rate of plants. Using a logistic model with growth rate r and carrying capacity k, the final equation in the system above characterizes the intrinsic growth of Cercospora sojina in the soil. Furthermore, the term ξI denotes the entire reciprocal contribution per unit of time made by the infected plants to the ambient pathogen.

In recent decades, many researchers from a variety of fields have become interested in the theory of fractional calculus. Fractional derivatives are a very useful tool for modeling a wide range of engineering science problems. We address a variety of definition types in the sections that follow.

Definition 1. Let Y be defined on $L^1([0.t], R)$, then we define the Riemann Liouville integral (Li et al., 2011) by

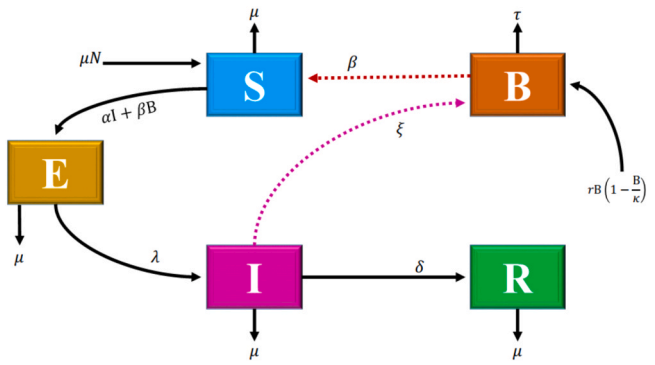

Fig. 1. Flowchart of dynamical system. FLS dynamics are partitioned into deterministic and fractal-fractional scenarios, driven by biological factors, reflecting the progression of infection stages.

$$ {}^{RL}_{0}I t^{\nu} Y(t) = \frac{1}{\Gamma(\nu)} \int_0^t (t-\xi)^{\nu-1} Y(\xi) d\xi, \tag{2} $$

where integral is point-wise defined on $(0, \infty)$ and $\nu \epsilon (0, 1]$.

Definition 2.2. The Caputo derivative of Y is given (Li et al., 2011) by

$$ {}^{RL}_{0}D t^{\nu} Y(t) = \frac{1}{\Gamma(n-\nu)} \left[\int_0^t (t-\xi)^{n-\nu-1} \frac{d^n}{d\xi^n} Y(t)(\xi) d\xi \right], \tag{3} $$

where $\Gamma(.)$ Represents the Gamma function. At $n = 1$,

$$ {}^{RL}_{0}D t^{\nu} Y(t) = \frac{1}{\Gamma(1-\nu)} \left[\int_0^t (t-\xi)^{-\nu} \frac{d}{d\xi} Y(t)(\xi) d\xi \right]. \tag{4} $$

Fractional differential operators are non-local and consider past state of a disease. It helps in enhancing disease transmission dynamics, long-term forecasts, and control and management strategies. The behavior of epidemiological models using different kinds of fractional operators has been investigated in a number of studies. As a result, the modified system in the frame of the arbitrary-order Caputo derivative is as follows:

$$ \begin{aligned} {}^{c}_{0}D^{\gamma}_{t} S(t) &= \mu N - (\alpha I + \beta B) S - \mu S, \\ {}^{c}_{0}D^{\gamma}_{t} E(t) &= \quad (\alpha I + \beta B) S - \mu E - \lambda E, \\ {}^{c}_{0}D^{\gamma}_{t} I(t) &= \lambda E - \mu I - \delta I, \\ {}^{c}_{0}D^{\gamma}_{t} R(t) &= \delta I - \mu R, \\ {}^{c}_{0}D^{\gamma}_{t} B(t) &= rB\left(1 - \frac{B}{k}\right) - \tau B + \xi I. \end{aligned} \tag{5} $$

The initial conditions are as follows:

$$ S(0) \geq 0, \quad E(0) \geq 0, \quad I(0) \geq 0, \quad R(0) \geq 0, \quad B(0) \geq 0. $$

Table 1
Proposed model parameters described.

Parameter	Description
μ	The plants' natural rate of growth and removal,
β	The primary infection transmission rate
α	The rates of transmission of secondary infections, respectively
λ	The mean latent period's reciprocal,
δ	The rate at which infectious plants are removed,
r	Intrinsic growth rate of fungi
κ	The fungus's carrying capacity
τ	The rate at which the fungus is removed from the soil
ξ	The typical rate at which an infectious plant contributes to the soil fungus

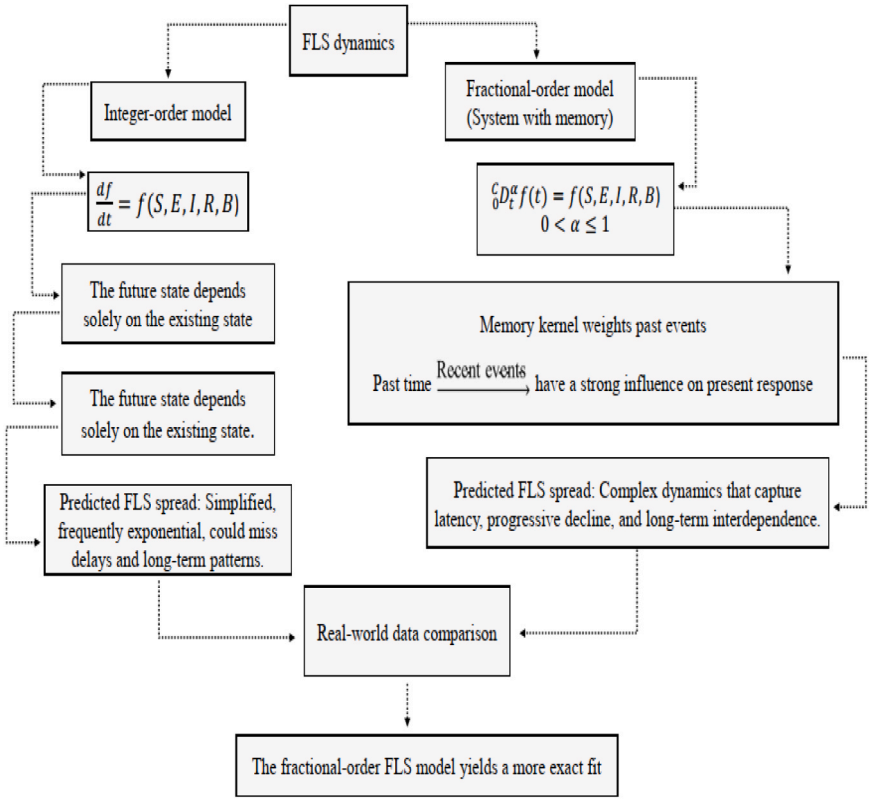

Fig. 2. Comparison of FLS dynamics influenced by integer and fractional order models.

All these parameters are taken to be positive. The flowchart of a dynamical system is depicted in Figs. 1 and 2. The description of parameters is given in Table 1.

3. Key analysis

3.1. Well-posedness

Because all system solutions for population-studied problems must remain non-negative and bounded. Therefore, establishing the positivity and boundedness of solutions will be essential. Consequently, we get the following results:

$$S(t) = \mu N - (\alpha I + \beta B)S - \mu S$$

$$\geq -(\alpha I + \beta B)S - \mu S$$

$$\geq -(\alpha I + \beta B + \mu)S$$

$$\geq -(\alpha |I| + \beta |B| + \mu)S$$

$$\geq -\left(\alpha \sup_{t\epsilon D_I} |I| + \beta \sup_{t\epsilon D_I} |B| + \mu\right)S$$

$$\geq -\left(\alpha \|I\|_\infty + \beta \|B\|_\infty + \mu\right)S$$

$$\mathrm{S(t)} \quad \geq S(0)E_\gamma[-\left(\alpha \|I\|_\infty + \beta \|B\|_\infty + \mu\right)t] \quad \forall \quad t \geq 0 \tag{6}$$

Similarly, we find

$$E(t) \quad \geq E(0)E_\gamma[-(\mu + \lambda)t], \tag{7}$$

$$\mathrm{I(t)} \geq I(0)E_\gamma[-(\mu + \delta)t], \tag{8}$$

$$R(t) \geq R(0)E_\gamma[-(\mu)t], \tag{9}$$

$$B(t) \geq B(0)E_\gamma\left[-\left(\frac{r\|B\|_\infty}{k} + \tau\right)t\right]. \tag{10}$$

3.2. Existence and uniqueness

Consider the system as

$$G_1 = (t, S_h, E, I_m, R, B) = \mu N - (\alpha I + \beta B)S - \mu S,$$

$$G_2 = (t, S_h, E, I_m, R, B) = (\alpha I + \beta B)S - \mu E - \lambda E,$$

$$G_3 = (t, S_h, E, I_m, R, B) = \lambda E - \mu I - \delta I$$

$$G_4 = (t, S_h, E, I_m, R, B) = \delta I - \mu R,$$

$$G_5 = (t, S_h, E, I_m, R, B) = rB\left(1 - \frac{B}{k}\right) - \tau B + \xi I. \tag{11}$$

Establish a Banach space $\mathrm{A}[0, T] = \mathrm{B}$ under the norm

$$\|G\| = \sup_{t\in[0,T]} [|S_h(t)| + |E(t)| + |I_m(t)| + |R_s(t)| + |B(t)|],$$

$$\varpi(t) = \{S(t), E(t), I(t), R(t), B(t)\}^T,$$

$$\varpi(0) = \{S(0), E(0), I(0), R(0), B(0)\}^T.$$

From the aforementioned collection, we can donate the system as

$${}_0^c D_t^\gamma = \omega(t, \Psi(t)) \quad , \quad t \in [0, T],$$

$$\Psi(0) = \Psi_0.$$

The above equation can be expressed as follows:

$$\Psi(0) = \Psi_0 + \frac{1}{\Gamma(\gamma)} \int_0^t (t - \zeta)^{\gamma - 1} \omega(\zeta, \Psi(\zeta) d\zeta,$$

The following presumptions are made to demonstrate that the solution exists:

$\{Y_1\} : \exists$ constants$X_k, X_m > 0$ such that
$|\omega(t, \Psi(t))| \leq X_k |\Psi(t)|^\omega + X_m.$
$\{Y_1\}$: For each$\Psi_1, \Psi_2 \exists$ constant$X_L > 0$ such that

$$|\omega(t, \Psi_1(t))| - |\omega(t, \Psi_2(t))| \leq \|\Psi_1(t) - \Psi_2(t)\|.$$

Establish an operator $\mathfrak{S} : \mathscr{B}to\mathscr{B}$as

$$\mathfrak{S}^{\Psi_1(t)} = \Psi_0 + \frac{1}{\Gamma(\gamma)} \int_0^t (t - \zeta)^{\gamma - 1} \omega(\zeta, \Psi(\zeta) d\zeta. \tag{12}$$

4. Qualitative analysis

4.1. Equilibrium points

To find the equilibrium points, we set the RHS of system (5) equal to 0 as:

$$\mu N - (\alpha I + \beta B)S - \mu S = 0,$$

$$(\alpha I + \beta B)S - \mu E - \lambda E = 0,$$

$$\lambda E - \mu I - \delta I = 0,$$

$$\delta I - \mu R = 0,$$

$$rB\left(1 - \frac{B}{k}\right) - \tau B + \xi I = 0. \tag{13}$$

Disease-free equilibrium points:

$$P^0\left(S^0, E^0, I^0, R^0, B^0\right) = (N, 0, 0, 0, 0) \tag{14}$$

Endemic equilibrium points:

$$P_2(S^*, E^*, I^*, R^*, B^*) \tag{15}$$

We calculate endemic equilibrium points as

$$S^* = \frac{\mu N}{\alpha I^* + \beta B^* + \mu} E^* = \frac{(\alpha I^* + \beta B^*)S^*}{(\mu + \lambda)} = \frac{\lambda E^*}{\mu + \delta}, \quad R^* = \frac{\delta I^*}{\mu}, \quad B^* = \frac{\xi I^*}{\tau - r}$$

4.2. Reproductive number

Consider the system below:

$${}_0^c D_t^\gamma E(t) = \quad (\alpha I + \beta B)S - \mu E - \lambda E,$$

$${}_0^c D_t^\gamma I(t) = \lambda E - \mu I - \delta I,$$

$${}_0^c D_t^\gamma B(t) = rB\left(1 - \frac{B}{k}\right) - \tau B + \xi I. \tag{16}$$

We use next next-generation matrix method (Van den Driessche, 2017) as:

$$\mathrm{F} = \begin{pmatrix} 0 & \alpha S^0 & \beta S^0 \\ 0 & 0 & 0 \\ 0 & 0 & 0 \end{pmatrix} V = \begin{pmatrix} \mu + \lambda & 0 & 0 \\ \lambda & \mu + \delta & 0 \\ 0 & -\xi & \tau - r \end{pmatrix},$$

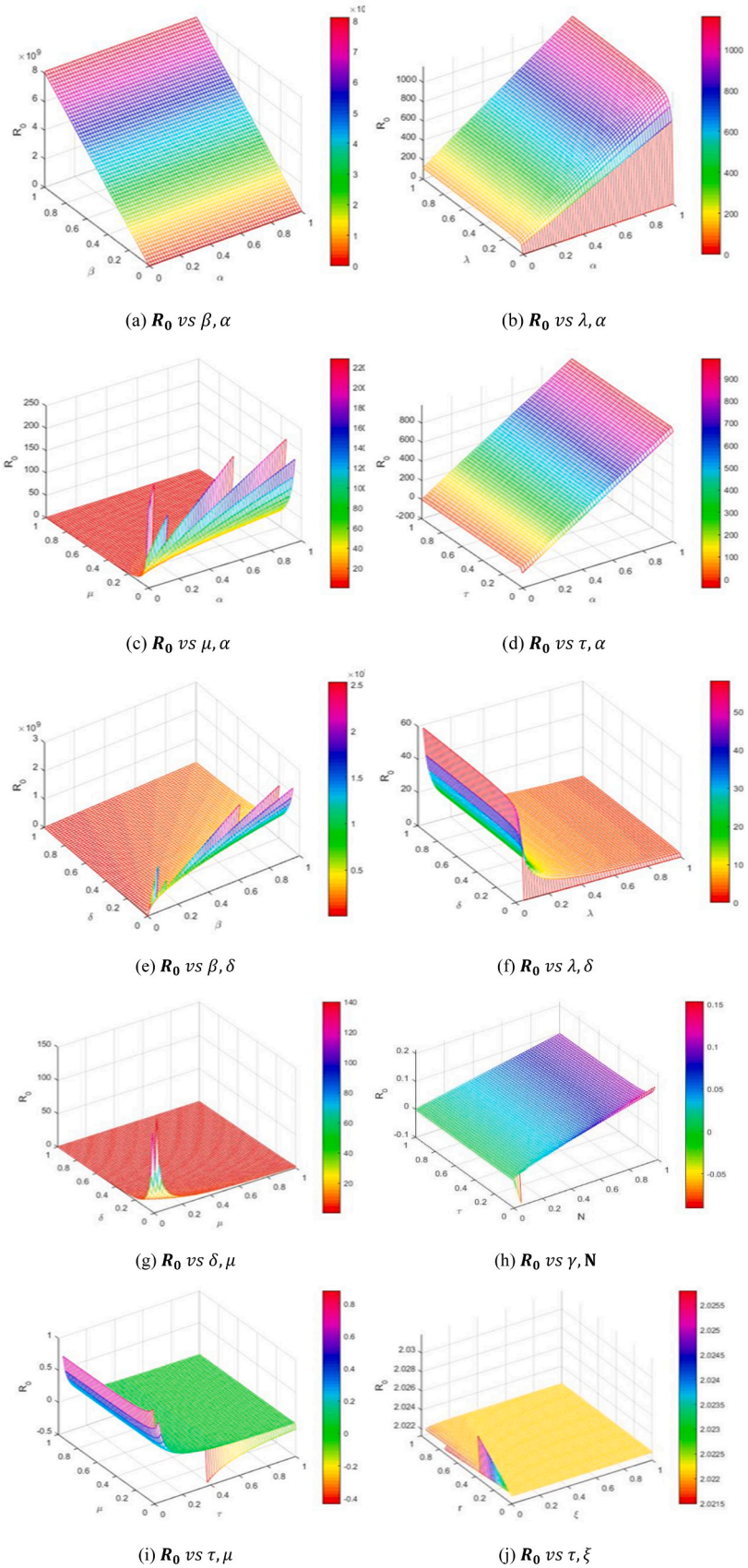

(a) $\boldsymbol{R_0}$ vs β, α (b) $\boldsymbol{R_0}$ vs λ, α

(c) $\boldsymbol{R_0}$ vs μ, α (d) $\boldsymbol{R_0}$ vs τ, α

(e) $\boldsymbol{R_0}$ vs β, δ (f) $\boldsymbol{R_0}$ vs λ, δ

(g) $\boldsymbol{R_0}$ vs δ, μ (h) $\boldsymbol{R_0}$ vs $\gamma, \mathbf{N}$

(i) $\boldsymbol{R_0}$ vs τ, μ (j) $\boldsymbol{R_0}$ vs τ, ξ

Fig. 3. Sensitivity of reproductive number's parameters.

$$V^{-1} = \begin{pmatrix} \frac{1}{\mu+\lambda} & 0 & 0 \\ -\frac{\lambda}{(\mu+\lambda)(\mu+\delta)} & \frac{1}{\mu+\delta} & 0 \\ \frac{\lambda\xi}{(\mu+\lambda)(\mu+\delta)(\tau-r)} & \frac{\lambda}{(\mu+\delta)(\tau-r)} & \frac{1}{\tau-r} \end{pmatrix},$$

$$FV^{-1} = \begin{pmatrix} \frac{\alpha N\lambda}{(\mu+\lambda)(\mu+\delta)} - \frac{\beta N\lambda\xi}{(\mu+\lambda)(\mu+\delta)[rB^2\left(1-\frac{B}{\kappa}\right)+\tau]} & \frac{\alpha s}{\mu+\delta} - \frac{\beta N\lambda}{(\mu+\lambda)(\mu+\delta)[rB^2\left(1-\frac{B}{\kappa}\right)+\tau]} & \frac{\beta N}{[rB^2\left(1-\frac{B}{\kappa}\right)+\tau]} \\ 0 & 0 & 0 \\ 0 & 0 & 0 \end{pmatrix},$$

From $\left|FV^{-1} - \lambda I\right| = 0$, we get the reproductive number as follows:

$$\boldsymbol{R}_0 = \frac{\alpha N\lambda(\tau-r) + \beta N\lambda\xi}{(\mu+\lambda)(\mu+\delta)(\tau-r)} \tag{17}$$

4.3. Sensitivity analysis

Reproductive number sensitivity testing is done. The goal of this analysis is to determine the influence of each model parameter as indicated by the sensitivity index.

$$\frac{\partial \boldsymbol{R}_0}{\partial\alpha} = \frac{N\lambda(\tau-r)+\beta N\lambda\xi}{(\mu+\lambda)(\mu+\delta)(\tau-r)} > 0 \frac{\partial \boldsymbol{R_0}}{\partial N} = \frac{\alpha\lambda(\tau-r)+\beta\lambda\xi}{(\mu+\lambda)(\mu+\delta)(\tau-r)} > 0$$

$$\frac{\partial \boldsymbol{R_0}}{\partial\beta} = \frac{N\lambda\xi}{(\mu+\lambda)(\mu+\delta)(\tau-r)} > 0 \frac{\partial \boldsymbol{R_0}}{\partial\xi} = \frac{\beta N\lambda}{(\mu+\lambda)(\mu+\delta)(\tau-r)} > 0$$

$$\frac{\partial \boldsymbol{R_0}}{\partial t} = -\frac{\beta N\lambda\xi}{(\mu+\lambda)(\mu+\delta)(\tau-r)^2} < 0 \quad \frac{\partial \boldsymbol{R_0}}{\partial r} = \frac{\beta N\lambda\xi}{(\mu+\lambda)(\mu+\delta)(\tau-r)^2} > 0$$

$$\frac{\partial \boldsymbol{R_0}}{\partial\mu} = -\frac{(\alpha N\lambda(\tau-r)+\beta N\lambda\xi)(2\mu+\lambda+\delta)}{(\mu+\lambda)^2(\mu+\delta)^2(\tau-r)^2} < 0, \tag{18}$$

$$\frac{\partial \boldsymbol{R_0}}{\partial\delta} = -\frac{\alpha N\lambda(\tau-r)+\beta N\lambda\xi}{(\mu+\lambda)(\mu+\delta)^2(\tau-r)} < 0 \frac{\partial \boldsymbol{R_0}}{\partial\lambda} = \frac{\alpha N\mu(\tau-r)+\beta N\xi\mu}{(\mu+\lambda)^2(\mu+\delta)(\tau-r)} > 0 \quad .$$

When the index is positive, it means that raising the parameter makes $\boldsymbol{R_0}$ larger; when it is negative, it means that raising the parameter makes $\boldsymbol{R_0}$ smaller.

Fig. 3 depicts how sensitive the basic reproductive number is to its factors. These graphs illustrate that $\boldsymbol{R_0}$ grows as parameters α, β, N, ξ or λ increases, whereas $\boldsymbol{R_0}$ decreases as parameters τ, μ or δ increases. Controlling primary and secondary contact rates (α and β) will reduce $\boldsymbol{R_0}$, hence lowering the incidence of FLS. Also, increasing the rate (τ) at which the fungus is removed from the soil will help to reduce the FLS outbreak.

5. Stability analysis

5.1. Local stability

Theorem 1. Disease free equilibrium point $P^0\left(S^0, E^0, I^0, R^0, B^0\right)$ is stable if $\boldsymbol{R}_0 < 1$.

$$\frac{dS}{dt} = \mu N - (\alpha I + \beta B)S - \mu S,$$

$$\frac{dE}{dt} = (\alpha I + \beta B)S - \mu E - \lambda E,$$

$$\frac{dI}{dt} = \lambda E - \mu I - \delta I,$$

$$\frac{dR}{dt} = \delta I - \mu R, \tag{1}$$

$$\frac{dB}{dt} = rB\left(1-\frac{B}{k}\right) - \tau B + \xi I.$$

Proof. Jacobian matrix of the system

$$\begin{pmatrix} -\alpha I - \beta B - \mu 0 & -\alpha S & 0 & -\beta S \\ \alpha I + \beta B & -\mu - \lambda\alpha S & 0 & \beta S \\ 0 & \lambda - \mu - \delta & 0 & 0 \\ 0 & 0 & \delta - \mu & 0 \\ 0 & 0 & \xi & 0 \end{pmatrix} \begin{matrix} \\ \\ \\ \\ -r - \frac{2Br}{k} + \tau \end{matrix} \tag{19}$$

Jacobian matrix at P^0

$$J\left(P^0\right) = \begin{pmatrix} -\mu & 0 & -\alpha N & 0 & -\beta N \\ 0 & -\mu - \lambda\alpha N & 0 & \beta N & \\ 0 & \lambda - \mu - \delta & 0 & 0 & \\ 0 & 0 & \delta - \mu & 0 & \\ 0 & 0 & \xi & 0 & -r+\tau \end{pmatrix} \tag{20}$$

We can write the characteristic equation as

$$f_{(q)} = \begin{pmatrix} -\mu - q & 0 & -\alpha N & 0 & -\beta N \\ 0 & -\mu - \lambda - q\alpha N & 0 & \beta N & \\ 0 & \lambda - \mu - \delta - q & 0 & 0 & \\ 0 & 0 & \delta - \mu - q & 0 & \\ 0 & 0 & \xi & 0 & -r+\tau-q \end{pmatrix} \tag{21}$$

We find

$$q_1 = -\mu q_2 = -\mu - \lambda q_3 = -\mu - \delta q_4 = -\mu q_5 = -r + \tau.$$

Since all eigenvalues are negative so P^0 is a locally stable point.

Theorem 2. Endemic equilibrium point $P_2(S^*, E^*, I^*, R^*, B^*)$ is stable if $\boldsymbol{R}_0 > 1$.

Proof. Jacobian matrix at P_2

$$J(P_2)=\begin{pmatrix} -\alpha\frac{\lambda E^*}{\mu+\delta}-\beta\frac{\xi I^*}{\tau-r}-\mu & 0 & -\frac{\alpha\mu N}{\alpha I^*+\beta B^*+\mu} & 0 & -\frac{\beta\mu N}{\alpha I^*+\beta B^*+\mu} \\ \alpha\frac{\lambda E^*}{\mu+\delta}+\beta\frac{\xi I^*}{\tau-r} & -\mu-\lambda & \frac{\alpha\mu N}{\alpha I^*+\beta B^*+\mu} & 0 & \frac{\beta\mu N}{\alpha I^*+\beta B^*+\mu} \\ 0 & \lambda & -\mu-\delta & 0 & 0 \\ 0 & 0 & \delta & -\mu & 0 \\ 0 & 0 & \xi & 0 & -r-\frac{2\frac{\xi I^*}{\tau-r}r}{k}+\tau \end{pmatrix} \tag{22}$$

We can write the characteristic equation as

$$f_{(q)}=\begin{pmatrix} -\alpha\frac{\lambda E^*}{\mu+\delta}-\beta\frac{\xi I^*}{\tau-r}-\mu-q & 0 & -\frac{\alpha\mu N}{\alpha I^*+\beta B^*+\mu} & 0 & -\frac{\beta\mu N}{\alpha I^*+\beta B^*+\mu} \\ \alpha\frac{\lambda E^*}{\mu+\delta}+\beta\frac{\xi I^*}{\tau-r} & -\mu-\lambda-q & \frac{\alpha\mu N}{\alpha I^*+\beta B^*+\mu} & 0 & \frac{\beta\mu N}{\alpha I^*+\beta B^*+\mu} \\ 0 & \lambda & -\mu-\delta-q & 0 & 0 \\ 0 & 0 & \delta & -\mu-q & 0 \\ 0 & 0 & \xi & 0 & -r-\frac{2\frac{\varepsilon I^*}{\tau-r}r}{k}+\tau-q \end{pmatrix} \tag{23}$$

$$q_1=-\alpha\frac{\lambda E^*}{\mu+\delta}-\beta\frac{\xi I^*}{\tau-r}-\mu \quad q_2=-\mu-\lambda \quad q_3=-\mu-\delta,$$

$$q_4=-\mu-q \quad q_5=-r-\frac{2\frac{\xi I^*}{\tau-r}r}{k}+\tau.$$

Since all eigenvalues are negative so P_2 is a locally stable point.

5.2. Global stability

For the endemic Lyapunov function, $\{S,E,I,R,B\}{}_0^cD_t^\gamma L<0$ is the endemic equilibrium P_2.

Theorem 3. P_2 of the model is globally asymptotically stable when $R_0>1$.

The proof Lyapunov function is as follows:

$$L=\left(S-S^*-S^*\ln\frac{S}{S^*}\right)\left(E-E^*-E^*\ln\frac{E}{E^*}\right)+\left(I-I^*-I^*\ln\frac{I}{i^*}\right)+\left(R-R^*-R^*\ln\frac{R}{R^*}\right)+\left(B-B^*-B^*\ln\frac{B}{B^*}\right) \tag{24}$$

Then

$${}_0^cD_t^\gamma L \le \left(\frac{S-S^*}{S^*}\right){}_0^cD_t^\gamma S+\left(\frac{E-E^*}{E^*}\right){}_0^cD_t^\gamma E+\left(\frac{I-I^*}{I^*}\right){}_0^cD_t^\gamma I+\left(\frac{R-R^*}{R^*}\right){}_0^cD_t^\gamma R+\left(\frac{B-B^*}{B^*}\right){}_0^cD_t^\gamma B \tag{25}$$

Also,

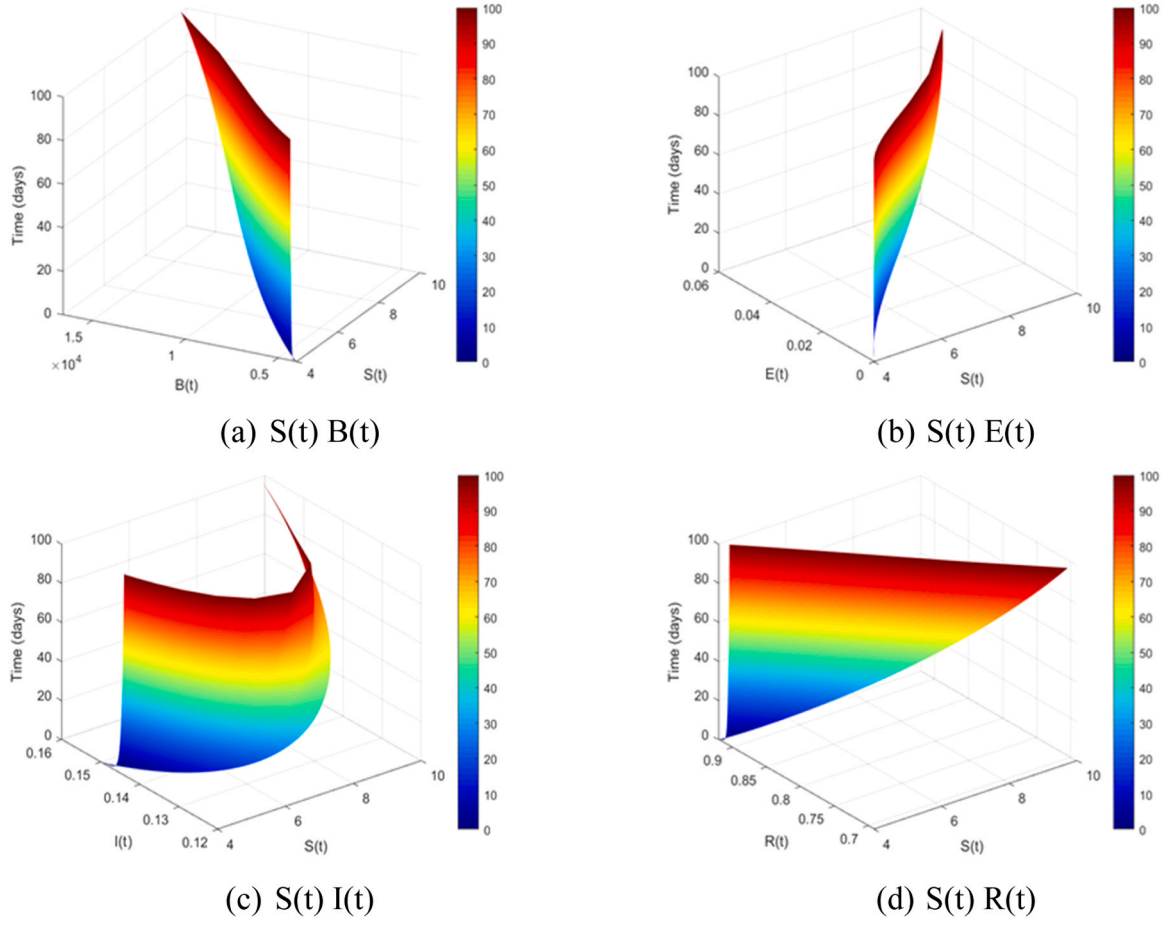

Fig. 4. Correlation of S(t) with other compartments at different fractional values.

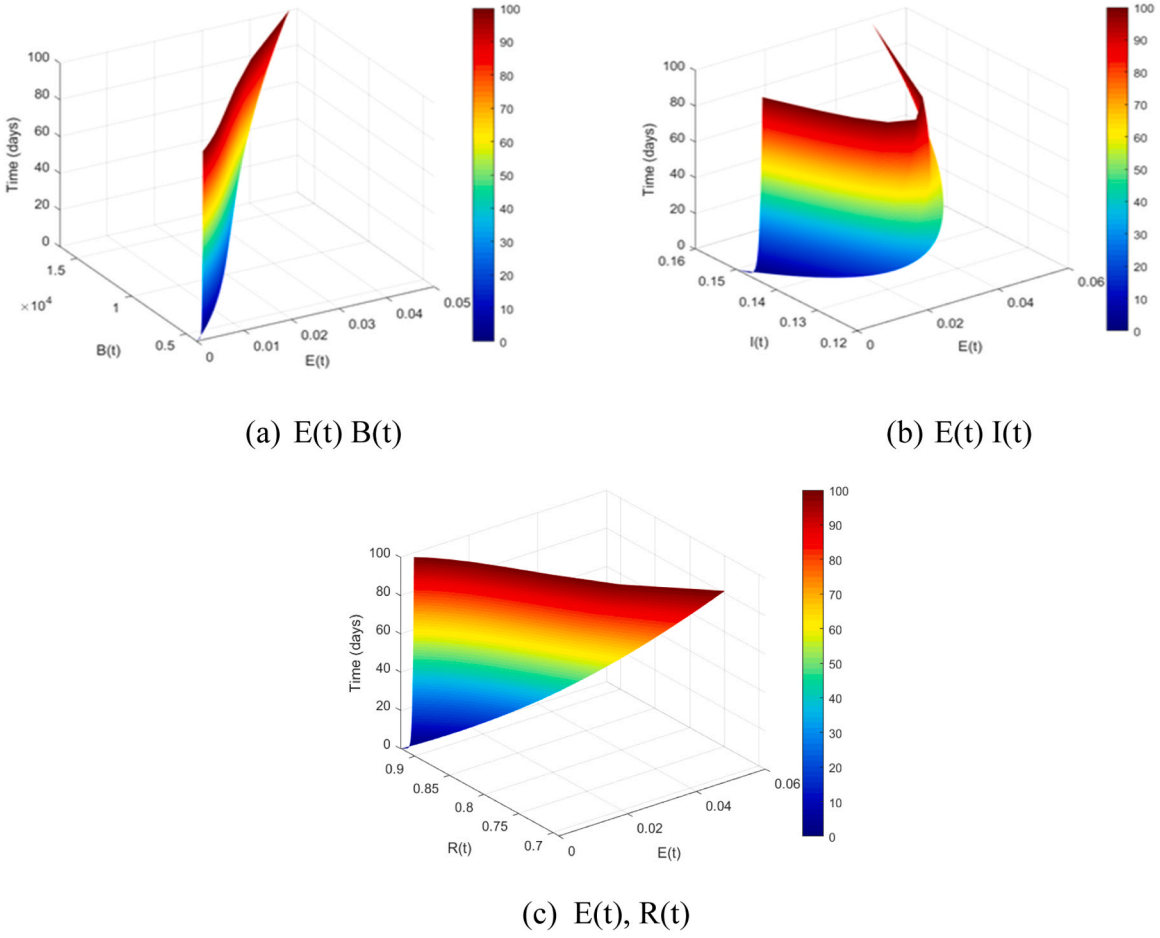

Fig. 5. Correlation of E(t) with other compartments at different fractional values.

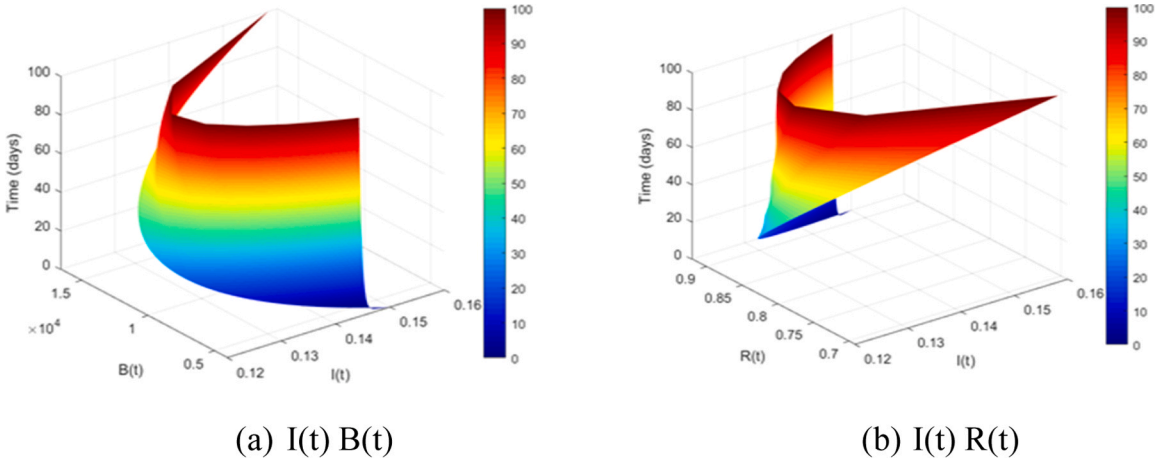

Fig. 6. Correlation of I(t) with other compartments at different fractional values.

$$
\begin{aligned}
{}_{0}^{c}D_{t}^{\gamma}L \leq \left(\frac{S-S^{*}}{S^{*}}\right)\ & (\mu N-(\alpha I+\beta B)S-\mu S)+\left(\frac{E-E^{*}}{E^{*}}\right)((\alpha I+\beta B)S \\
& -\mu E-\lambda E)+\left(\frac{I-I^{*}}{I^{*}}\right)(\lambda E-\mu I-\delta I)+\left(\frac{R-R^{*}}{R^{*}}\right)(\delta I-\mu R) \\
& +\left(\frac{\mathrm{B}-\mathrm{B}^{*}}{\mathrm{B}^{*}}\right)\left(rB\left(1-\frac{B}{k}\right)-\tau B+\xi I\right) \qquad (26)
\end{aligned}
$$

Let $S = S - S^{*}, E = E - E^{*}, I = I - I^{*}, R = R - R^{*}, B = B - B$

$$
\begin{aligned}
{}_{0}^{c}D_{t}^{\gamma}L \leq\ & \mu N-\alpha IS+\beta BS-\mu S-\frac{S^{*}}{S}\mu N+\frac{S^{*}}{S}\alpha IS-\frac{S^{*}}{S}\beta BS+\frac{S^{*}}{S}\mu S \\
& +\alpha IS+\beta BS-\mu E-\lambda E-\frac{E^{*}}{E}\alpha IS-\frac{E^{*}}{E}\beta BS+\frac{E^{*}}{E}\mu E+\frac{E^{*}}{E}\lambda E \\
& \lambda E-\mu I-\delta I-\frac{I^{*}}{I}\lambda E+\frac{I^{*}}{I}\mu I+\frac{I^{*}}{I}\delta I
\end{aligned}
$$

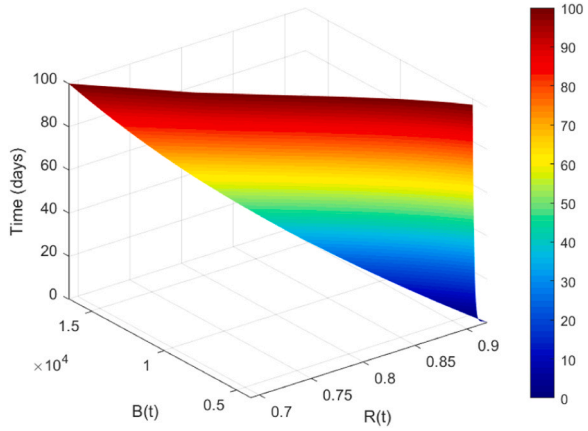

Fig. 7. Correlation of R(t) with B(t).

Table 2
Model parameter's values (Yang and Wang, 2023).

Parameters	Values	Units
N	21	Per square meter
μ	0.00666	Per day
λ	0.1	Per day
δ	0.0133	Per day
τ	0.00136	Per day
κ	60,000	Per ml
r	0.001	Per day
β	0.0000000135	Per day
α	0.00205	Per day
ξ	2960	Per day

$$+\delta I-\mu R-\frac{R^*}{R}\delta I+\frac{R^*}{R}\mu R$$

$$+rB-\frac{rB^2}{k}-\tau B+\xi I-\frac{B^*}{B}rB+\frac{B^*rB}{Bk}+\frac{B^*}{B}\tau B-\frac{B^*}{B}\xi I. \tag{27}$$

After some computations, we have

$${}_0^cD_t^\gamma L\le \Omega_1-\Omega_2$$

It is noted that if $\Omega_1<\Omega_2$, this yields ${}_0^cD_t^\gamma L<0$, however when

$S=S^*, S=S^*, E=E^*, I=I^*, R=R^*,$ and $B=B^*$.

$$0=\Omega_1-\Omega_2\Rightarrow\ {}_0^cD_t^\gamma L=0$$

In the invariant region if $\Omega_1<\Omega_2$, P_2 is thus globally asymptotically stable.

6. Chaos control

Examining a managed-design fractional-order system, system (5) is stabilized based on its equilibrium points by employing the linear feedback regulation technique.

$${}_0^cD_t^\gamma S(t)=\mu N-(\alpha I+\beta B)S-\mu S-\Theta_1\quad (S-S^*),$$

$${}_0^cD_t^\gamma E(t)=\quad (\alpha I+\beta B)S-\mu E-\lambda E-\Theta_2\quad (E-E^*),$$

$${}_0^cD_t^\gamma I(t)=\lambda E-\mu I-\delta I-\Theta_3\quad (I-I^*),$$

$${}_0^cD_t^\gamma R(t)=\delta I-\mu R-\Theta_4\quad (R-R^*), \tag{28}$$

$${}_0^cD_t^\gamma B(t)=rB\left(1-\frac{B}{k}\right)-\tau B+\xi I-\Theta_5\quad (B-B^*).$$

The control parameters and equilibria are denoted by $\Theta_1,\Theta_2,\Theta_3,\Theta_4,\Theta_5$, and S^*,E^*,I^*,R^*,B^*, respectively.

Jacobian matrix at P^0

$$J(P^0)\begin{pmatrix}-\mu-\Theta_1 & 0 & -\alpha N & 0 & -\beta N\\ 0 & -\mu-\lambda-\Theta_2\alpha N & 0\beta N & & \\ & 0\lambda-\mu-\delta-\Theta_3 & 00 & & \\ & 00\delta-\mu-\Theta_1 & 0 & & \\ & 00\xi 0 & -r+\tau-\Theta_5 & & \end{pmatrix}.$$

We can write the characteristic equation as

$$f(q)=\begin{pmatrix}-\mu-q-\Theta_1 & 0 & -\alpha N & 0 & -\beta N\\ 0 & -\mu-\lambda-q-\Theta_2\alpha N & 0\beta N & & \\ & 0\lambda-\mu-\delta-q & -\Theta_3 & 00 & \\ & 00\delta-\mu-q-\Theta_4 & 0 & & \\ & 00\xi 0 & -r+\tau-q-\Theta_5 & & \end{pmatrix}.$$

Eigenvalues are

$$q_1=-\mu-\Theta_1,$$

$$q_{\ 2}=-\mu-\lambda-\Theta_2,$$

$$q_3=-\mu-\delta-\Theta_3,$$

$$q_4=-\mu-\Theta_4,$$

$$q_5=-r+\tau-\Theta_5.$$

Let $\Theta_1=1$, $\Theta_2=2$, $\Theta_3=3$, $\Theta_4=4$ and $\Theta_5=5$, then

$$q_1=-\mu-1,$$

$$q_2=-\mu-\lambda-2,$$

$$q_3=-\mu-\delta-3,$$

$$q_4=-\mu-4,$$

$$q_5=-r+\tau-5. \tag{29}$$

Since all eigenvalues are negative so P^0 is a locally stable point (Figs. 4–7).

7. Numerical scheme

The literature indicates that the best model for simulating power law processes in practical settings is the Caputo derivative. For ease of use, we will write the aforementioned system as follows:

$$H_1(S_h,E,I_m,R_s,B)=\mu N-(\alpha I+\beta B)S-\mu S,$$

$$H_2(S_h,E,I_m,R_s,B)=(\alpha I+\beta B)S-\mu E-\lambda E,$$

$$H_3(S_h,E,I_m,R_s,B)=\lambda E-\mu I-\delta I, \tag{30}$$

$$H_4(S_h,E,I_m,R_s,B)=\delta I-\mu R,$$

$$H_5(S_h,E,I_m,R_s,B)=rB(1-\frac{B}{\kappa})-\tau B+\zeta I,$$

After applying the fractional integral, we have the following:

$$S_h(t_k+1)=S_h(0)+\frac{1}{\Gamma(\gamma)}\sum_{i=2}^{k}\int_{t_i}^{t_{i+1}}H_1(S_h,E,I_m,R_s,B)(t_{k+1}-\psi)^{\gamma-1}d\psi,$$

$$E(t_k+1)=E(0)+\frac{1}{\Gamma(\gamma)}\sum_{i=2}^{k}\int_{t_i}^{t_{i+1}}H_2(S_h,E,I_m,R_s,B)(t_{k+1}-\psi)^{\gamma-1}d\psi,$$

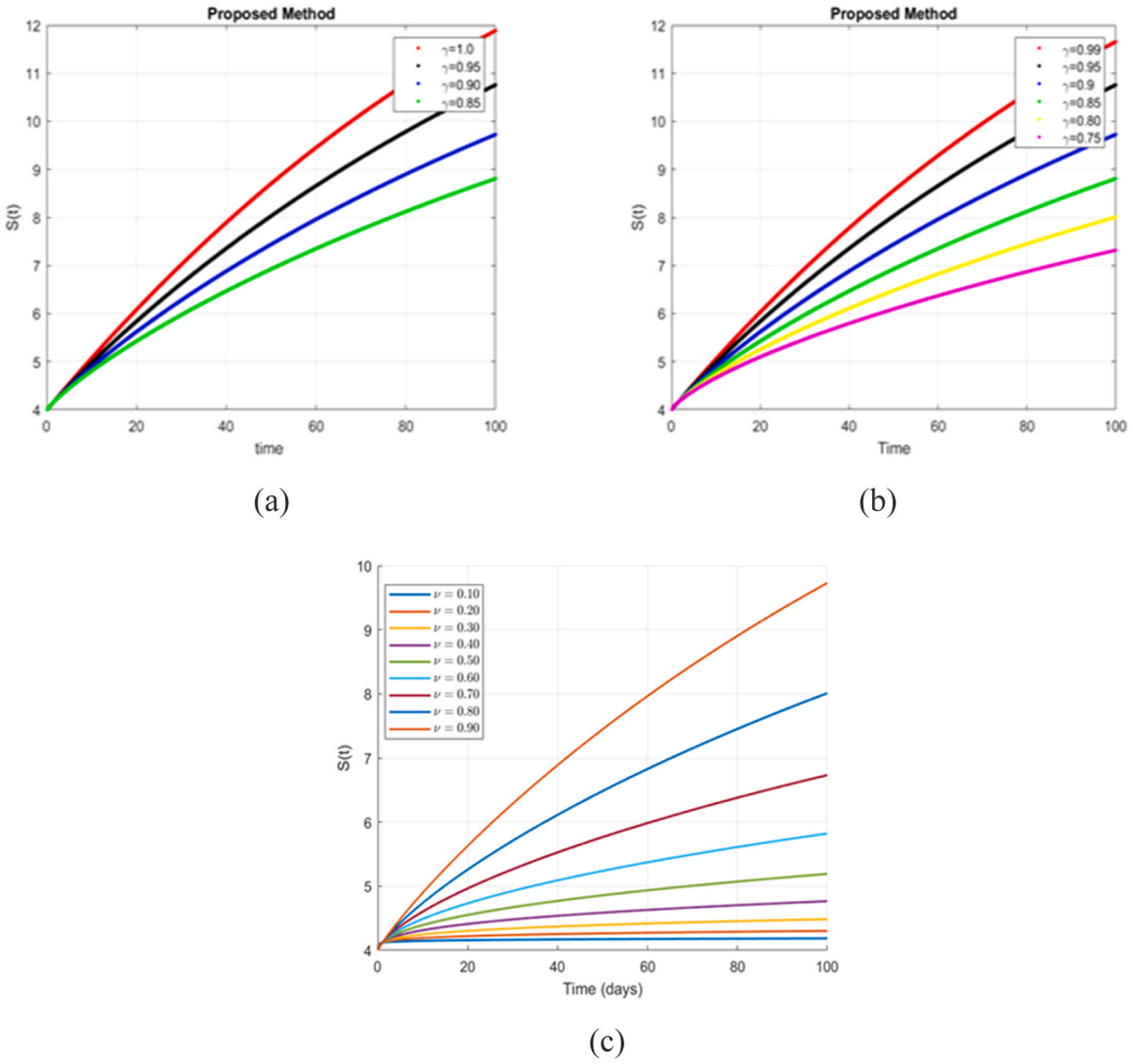

Fig. 8. Simulation of S(t) at different fractional and integer orders.

$$I_m(t_k+1) = I_m(0) + \frac{1}{\Gamma(\gamma)} \sum_{i=2}^{k} \int_{t_i}^{t_{i+1}} H_3(S_h, E, I_m, R_s, B)(t_{k+1} - \psi)^{\gamma-1} d\psi, \tag{31}$$

$$R_s(t_k+1) = R_s(0) + \frac{1}{\Gamma(\gamma)} \sum_{i=2}^{k} \int_{t_i}^{t_{i+1}} H_4(S_h, E, I_m, R_s, B)(t_{k+1} - \psi)^{\gamma-1} d\psi,$$

$$B(t_k+1) = B(0) + \frac{1}{\Gamma(\gamma)} \sum_{i=2}^{k} \int_{t_i}^{t_{i+1}} H_5(S_h, E, I_m, R_s, B)(t_{k+1} - \psi)^{\gamma-1} d\psi,$$

Here, we recall the Newton polynomial as follows:

$$P(t, S_h, E, I_m, R_s, B)$$

$$\cong P(t_{k-2}, S_h^{k-2}, E^{k-2}, I_m^{k-2}, R_s^{k-2}, B^{k-2})$$

$$+\frac{1}{\Delta t}\{P(t_{k-1}, S_h^{k-1}, E^{k-1}, I_m^{k-1}, R_s^{k-1}, B^{k-1}) - P(t_{k-2}, S_h^{k-2}, E^{k-2}, I_m^{k-2}, R_s^{k-2}, B^{k-2})\}$$

$$\times(\zeta - t_{k-2}) + \frac{1}{2\Delta t^2}\{t_k, S_h^k, E^k, I_m^k, R_s^k, B^k\} - 2P(t_{k-2}, S_h^{k-1}, E^{k-1}, I_m^{k-1}, R_s^{k-1}, B^{k-1})$$

$$+ P(t_{k-2}, S_h^{k-2}, E^{k-2}, I_m^{k-2}, R_s^{k-2}, B^{k-2}) \times (\zeta - t_{k-2})(\zeta - t_{k-1}). \tag{32}$$

Now, after the replacement of equations, we have for class S_h:

$$S_{h(k+1)} = S_h(0) + \frac{1}{\Gamma(\gamma)} \sum_{i=2}^{k} H_1(t_{i-2}, S_h^{i-2}, E^{i-2}, I_m^{i-2}, R_s^{i-2}, B^{i-2})$$

$$\times \int_{t_i}^{t_{i+1}} (t_{k+1} - \zeta)^{\gamma-1} d\zeta + \frac{1}{\Gamma(\gamma)} \sum_{i=2}^{k} \frac{1}{\Delta t}\{H_1(t_{i-1}, S_h^{i-1}, E^{i-1}, I_m^{i-1}, R_s^{i-1}, B^{i-1})\}$$
$$- H_1(t_{i-2}, S_h^{i-2}, E^{i-2}, I_m^{i-2}, R_s^{i-2}, B^{i-2})$$

$$\times \int_{t_i}^{t_{i+1}} (\zeta - t_{i-2})(t_{k+1} - \zeta)^{\gamma-1} d\zeta + \frac{1}{\Gamma(\gamma)} \sum_{i=2}^{k} \frac{1}{2\Delta t^2}\{H_1(t_i, S_h^i, E^i, I_m^i, R_s^i, B^i\}$$

$$- 2H_1(t_{i-1}, S_h^{i-1}, E^{i-1}, I_m^{i-1}, R_s^{i-1}, B^{i-1}) + H_1(t_{i-2}, S_h^{i-2}, E^{i-2}, I_m^{i-2}, R_s^{i-2}, B^{i-2})$$

$$\times \int_{t_i}^{t_{i+1}} (\zeta - t_{i-2})(\zeta - t_{i-1})(t_{k+1} - \zeta)^{\gamma-1} d\zeta. \tag{33}$$

Hence, we finally get

$$S_{h(k+1)} = S_h(0) + \frac{(\Delta t)^\gamma}{\Gamma(\gamma+1)} \sum_{i=2}^{k} H_1(t_{i-2}, S_h^{i-2}, E^{i-2}, I_m^{i-2}, R_s^{i-2}, B^{i-2}) \times \wedge_1$$

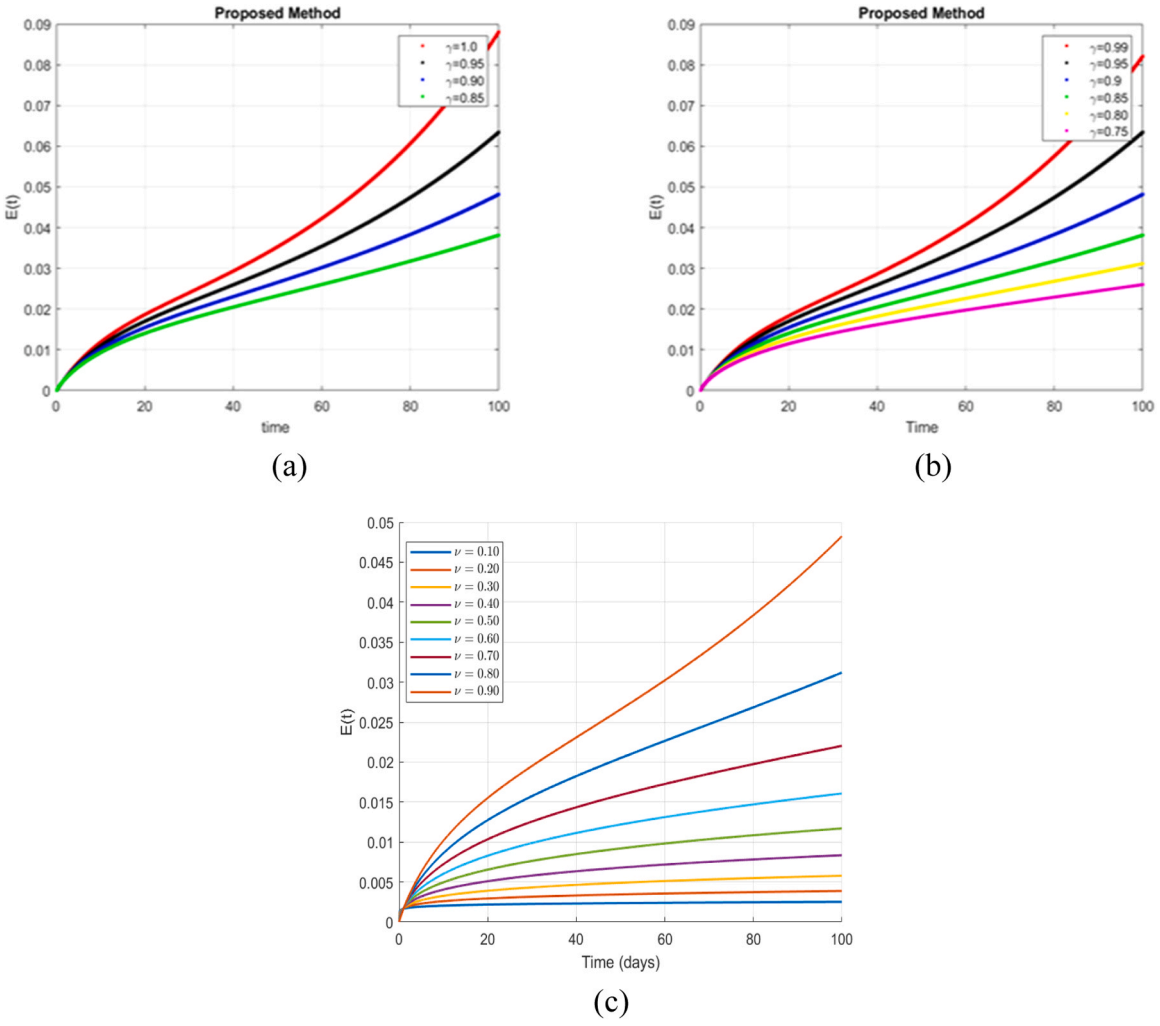

Fig. 9. Simulation of E(t) at different fractional and integer orders.

$$+\frac{(\Delta t)^{\gamma}}{\Gamma(\gamma+1)}\sum_{i=2}^{k}H_1(t_{i-1},S_h^{i-1},E^{i-1},I_m^{i-1},R_s^{i-1},B^{i-1})$$
$$-H_1(t_{i-2},S_h^{i-2},E^{i-2},I_m^{i-2},R_s^{i-2},B^{i-2})\times\wedge_2$$

$$+\frac{\gamma(\Delta t)^{\gamma}}{2\Gamma(\gamma+3)}\sum_{i=2}^{k}H_1(t_i,S_h^{i},E^{i},I_m^{i},R_s^{i},B^{i})-2H_1(t_{i-1},S_h^{i-1},E^{i-1},I_m^{i-1},R_s^{i-1},B^{i-1})$$

$$+H_1(t_{i-2},S_h^{i-2},E^{i-2},I_m^{i-2},R_s^{i-2},B^{i-2})\times\wedge_3, \tag{34}$$

where

$$\wedge_1=(\mathrm{k}-\mathrm{i}+1)^{\Psi}-(\mathrm{k}-\mathrm{i})^{\Psi},$$

$$\wedge_2=(\mathrm{k}-\mathrm{i}+1)^{\gamma}(\mathrm{k}-\mathrm{i}+3+2\gamma)-(\mathrm{k}-\mathrm{i})^{\gamma}(\mathrm{k}-\mathrm{i}+3+3\gamma),$$

$$\wedge_3=(\mathrm{k}-\mathrm{i}+1)^{\gamma}\left[\left\{2(\mathrm{k}-\mathrm{i})^2+(3\gamma+10)(\mathrm{k}-\mathrm{i})+2\gamma^2+9\gamma+12\right\}\right]$$

$$-(\mathrm{k}-\mathrm{i})^{\gamma}\left\{2(\mathrm{k}-\mathrm{i})^2+(5\gamma+10)(\mathrm{k}-\mathrm{i})+6\gamma^2+18\gamma+12\right\}.$$

$$E_{(t_{k+1})}=E(0)+\frac{(\Delta t)^{\gamma}}{\Gamma(\gamma+1)}\sum_{i=2}^{k}H_2(t_{i-2},S_h^{i-2},E^{i-2},I_m^{i-2},R_s^{i-2},B^{i-2})\times\wedge_1$$

$$+\frac{(\Delta t)^{\gamma}}{\Gamma(\gamma+1)}\sum_{i=2}^{k}H_2(t_{i-1},S_h^{i-1},E^{i-1},I_m^{i-1},R_s^{i-1},B^{i-1})-H_2(t_{i-2},S_h^{i-2},E^{i-2},I_m^{i-2},$$
$$R_s^{i-2},B^{i-2})\times\wedge_2$$

$$+\frac{\gamma(\Delta t)^{\gamma}}{2\Gamma(\gamma+3)}\sum_{i=2}^{k}H_2(t_i,S_h^{i},E^{i},I_m^{i},R_s^{i},B^{i})-2H_2(t_{i-1},S_h^{i-1},E^{i-1},I_m^{i-1},R_s^{i-1},B^{i-1})$$

$$+H_2(t_{i-2},S_h^{i-2},E^{i-2},I_m^{i-2},R_s^{i-2},B^{i-2})\times\wedge_3, \tag{35}$$

$$I_m(t_{k+1})=I_m(0)+\frac{(\Delta t)^{\gamma}}{\Gamma(\gamma+1)}\sum_{i=2}^{k}H_3(t_{i-2},S_h^{i-2},E^{i-2},I_m^{i-2},R_s^{i-2},B^{i-2})\times\wedge_1$$

$$+\frac{(\Delta t)^{\gamma}}{\Gamma(\gamma+1)}\sum_{i=2}^{k}H_3(t_{i-1},S_h^{i-1},E^{i-1},I_m^{i-1},R_s^{i-1},B^{i-1})$$
$$-H_3(t_{i-2},S_h^{i-2},E^{i-2},I_m^{i-2},R_s^{i-2},B^{i-2})\times\wedge_2$$

$$+\frac{\gamma(\Delta t)^{\gamma}}{2\Gamma(\gamma+3)}\sum_{i=2}^{k}H_3(t_i,S_h^{i},E^{i},I_m^{i},R_s^{i},B^{i})-2H_3(t_{i-1},S_h^{i-1},E^{i-1},I_m^{i-1},R_s^{i-1},B^{i-1})$$

$$+H_3(t_{i-2},S_h^{i-2},E^{i-2},I_m^{i-2},R_s^{i-2},B^{i-2})\times\wedge_3, \tag{36}$$

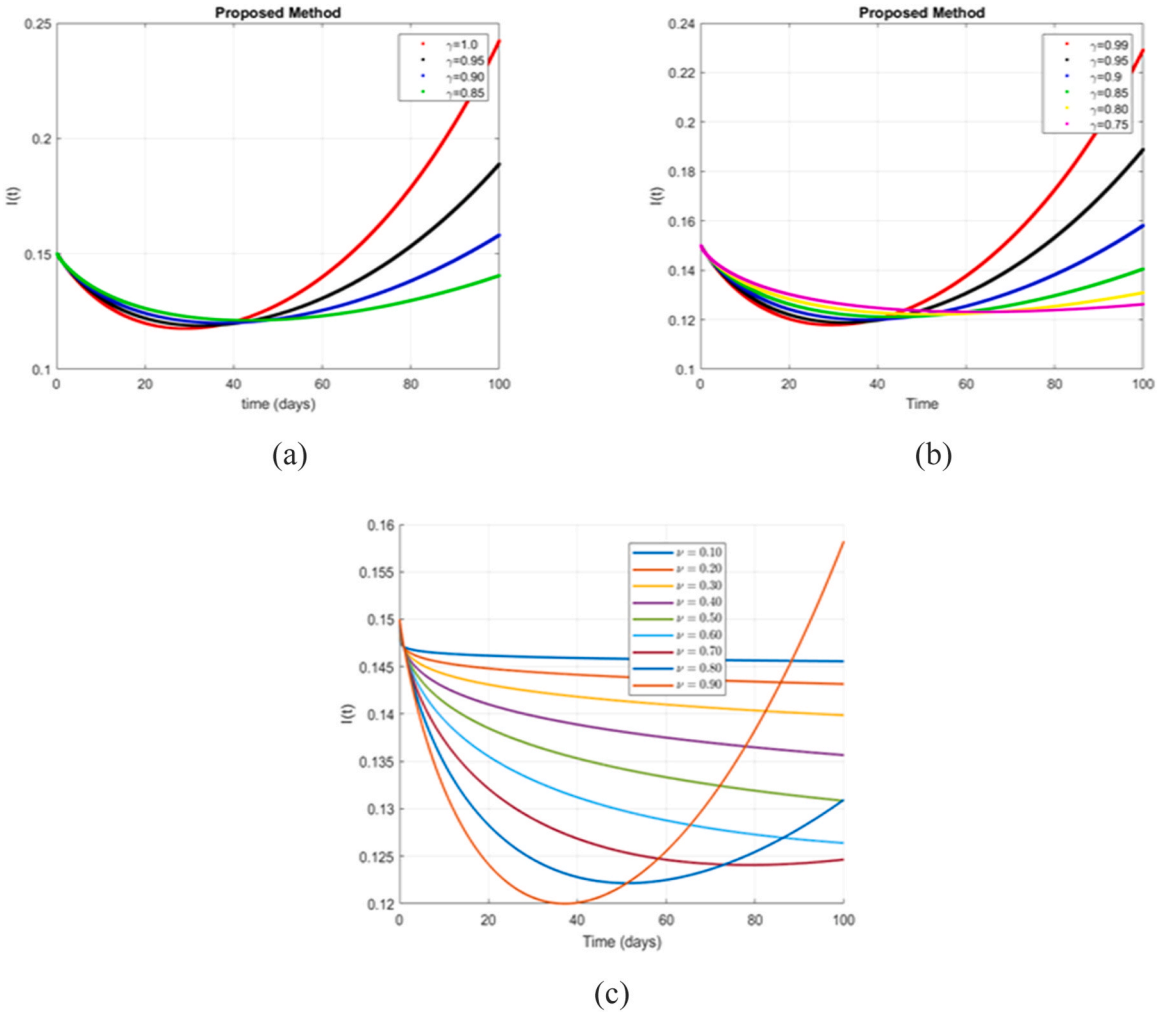

Fig. 10. Simulation of I(t) at different fractional and integer orders.

$$R_s(t_{k+1}) = I_s(0) + \frac{(\Delta t)^\gamma}{\Gamma(\gamma+1)} \sum_{i=2}^{k} H_4(t_{i-2}, S_h^{i-2}, E^{i-2}, I_m^{i-2}, R_s^{i-2}, B^{i-2}) \times \wedge_1$$

$$+ \frac{(\Delta t)^\gamma}{\Gamma(\gamma+1)} \sum_{i=2}^{k} H_4(t_{i-1}, S_h^{i-1}, E^{i-1}, I_m^{i-1}, R_s^{i-1}, B^{i-1})$$
$$- H_4(t_{i-2}, S_h^{i-2}, E^{i-2}, I_m^{i-2}, R_s^{i-2}, B^{i-2}) \times \wedge_2$$

$$+ \frac{\gamma(\Delta t)^\gamma}{2\Gamma(\gamma+3)} \sum_{i=2}^{k} H_4(t_i, S_h^i, E^i, I_m^i, R_s^i, B^i) - 2H_4(t_{i-1}, S_h^{i-1}, E^{i-1}, I_m^{i-1}, R_s^{i-1}, B^{i-1})$$

$$+ H_4(t_{i-2}, S_h^{i-2}, E^{i-2}, I_m^{i-2}, R_s^{i-2}, B^{i-2}) \times \wedge_3, \tag{37}$$

$$B(t_{k+1}) = B(0) + \frac{(\Delta t)^\gamma}{\Gamma(\gamma+1)} \sum_{i=2}^{k} H_5(t_{i-2}, S_h^{i-2}, E^{i-2}, I_m^{i-2}, R_s^{i-2}, B^{i-2}) \times \wedge_1$$

$$+ \frac{(\Delta t)^\gamma}{\Gamma(\gamma+1)} \sum_{i=2}^{k} H_5(t_{i-1}, S_h^{i-1}, E^{i-1}, I_m^{i-1}, R_s^{i-1}, B^{i-1})$$
$$- H_5(t_{i-2}, S_h^{i-2}, E^{i-2}, I_m^{i-2}, R_s^{i-2}, B^{i-2}) \times \wedge_2$$

$$+ \frac{\gamma(\Delta t)^\gamma}{2\Gamma(\gamma+3)} \sum_{i=2}^{k} H_5(t_i, S_h^i, E^i, I_m^i, R_s^i, B^i) - 2H_5(t_{i-1}, S_h^{i-1}, E^{i-1}, I_m^{i-1}, R_s^{i-1}, B^{i-1})$$

$$+ H_5(t_{i-2}, S_h^{i-2}, E^{i-2}, I_m^{i-2}, R_s^{i-2}, B^{i-2}) \times \wedge_3. \tag{38}$$

8. Findings and discussion

For mathematical analysis, the nonlinear frog eye leaf spot model of soybean disease has been suggested. The model's impact on treatment phases was confirmed through numerical computations based on parameter values from Yang and Wang (2023). In order to ensure a potential influence of variables, the effectiveness of the suggested frog eye leaf spot model was evaluated using the sophisticated Newton polynomial technique.

We used various fractional orders to simulate the compartments of the proposed system, as seen in the figures. By analyzing these figures, we can observe the impact of the Caputo fractional operator on the solutions of the current mathematical model.

Fig. 8 represents the simulation of S(t) at various fractional orders and integer values. As seen in Fig. 8(a)–(c), susceptible soybean leaves increase more rapidly at higher fractional orders.

Fig. 9 represents the simulation of E(t) at various fractional orders and integer values. As seen in Fig. 9(a)–(c), exposed soybean leaves increase more rapidly at higher fractional orders. Fig. 9 represents the simulation of I(t) at various fractional orders and integer values.

As seen in Fig. 10(a)–(c), the number of infected soybean leaves decreases and then increases again at higher fractional orders.

Fig. 11 represents the simulation of R(t) at various fractional orders and integer values. As seen in Fig. 11(a)–(c), recovered soybean leaves decrease more rapidly at higher fractional orders.

Fig. 12 represents the simulation of B(t) at various fractional orders

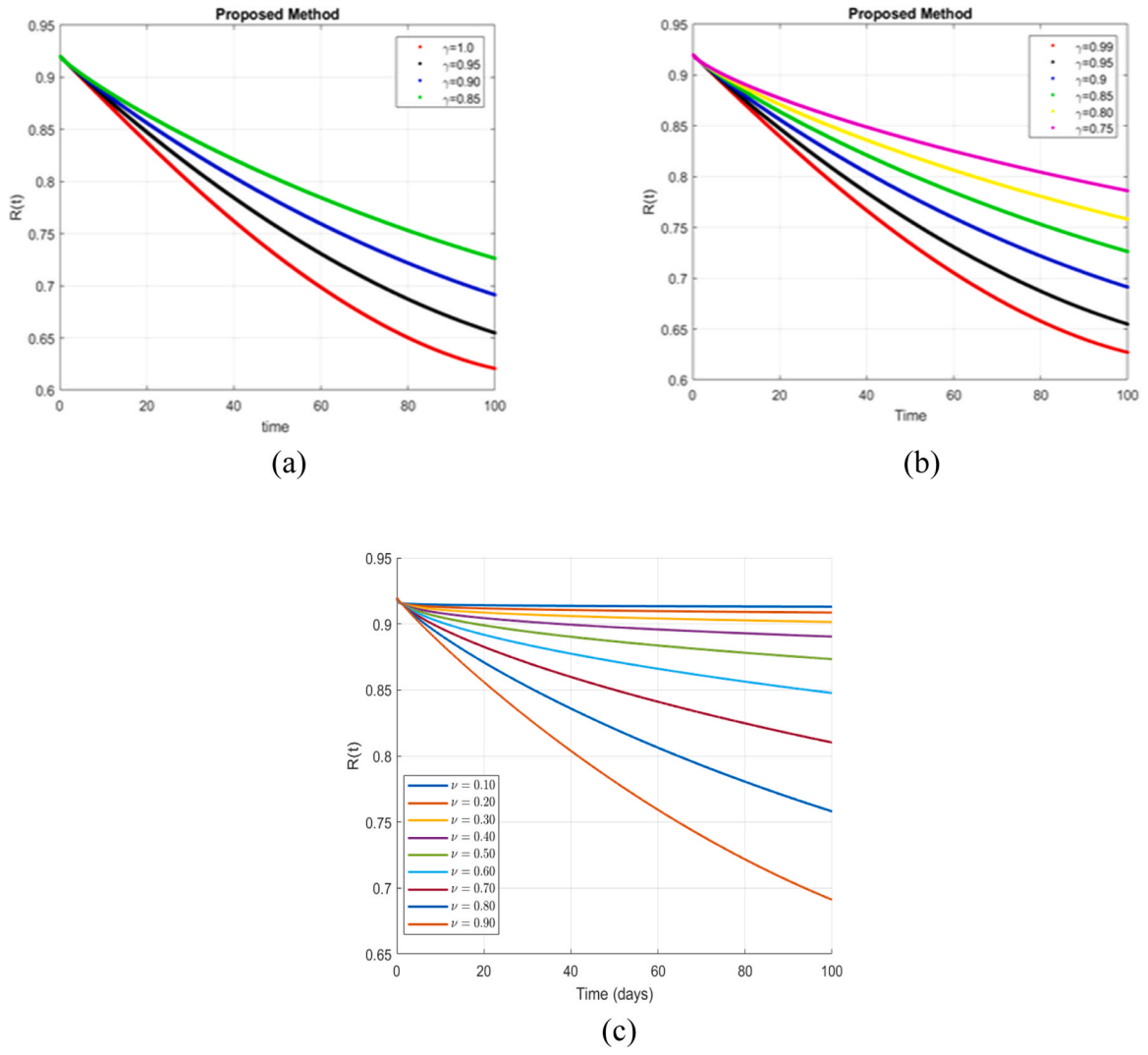

Fig. 11. Simulation of R(t) at different fractional and integer orders.

and integer values. As seen in Fig. 12(a)–(c), the fungus population on soybean leaves increases at higher fractional orders. Moreover, Figs. 13–17 represent the 3D surface and contour visualizations of the compartments of the proposed model at different fractional values.

The Newton polynomial serves as the foundation for our numerical solution to the system. The fractional derivative of the system's variables at discrete time points is approximated using the Newton polynomial interpolation. A function with a recursive advantage that computes its derivative at several points is called a Newton polynomial. When a new data point is added, only one new term needs to be added; all prior terms don't need to be recalculated. For fractional systems, Newton polynomial interpolation is an accurate technique that provides accurate numerical solutions. Because of its adaptability, it can be used with a variety of fractional derivatives and system types, such as fractal-fractional and chaotic models. The process is efficient because the recursive property makes adding new points easier. Newton polynomial interpolation provides incremental updates without recalculating the entire polynomial. This makes it a computationally efficient technique over Lagrange polynomials for solving fractional order systems. Predictor-corrector approaches, used to model complex systems with memory effects, benefit from this by efficiently constructing numerical formulas for fractional derivatives like Caputo and Atangana-Baleanu. For modeling and simulating complex systems in a variety of domains, including disease modeling, chaos, and complex systems, this numerical scheme is extremely helpful.

The results of the study provide a comprehensive analysis of the stability and dynamic behavior of frogeye leaf spot infections using a fractional-order mathematical model. The fractional order was varied from 0 to 1 in the simulations to observe the impact on the system dynamics. As it decreased, the infection rate that was getting close to equilibrium slowed significantly, indicating stronger memory effects. Disease management becomes complex in conditions influenced by past states, such as spore exposure or consistent weather, requiring long-term strategies over reactive interventions. In agricultural planning, monitoring and controlling low infection levels is crucial as they may accumulate over time without causing noticeable outbreaks. Based on the above explanation, we can predict that the disease will be eradicated by reducing infections in the future. For all classes at the Caputo operator, the numerical method constructed with Newton polynomials performs better than a traditional operator.

9. Conclusion

The dynamics and stability of frogeye leaf spot infections in soybean crops are investigated using fractional order operators. Combining the memory and genetic aspects of fractional calculus, particularly the Caputo derivative, provides a more precise and nuanced representation of the disease's behavior over time. The analysis revealed that the $\mathbf{R_0}$

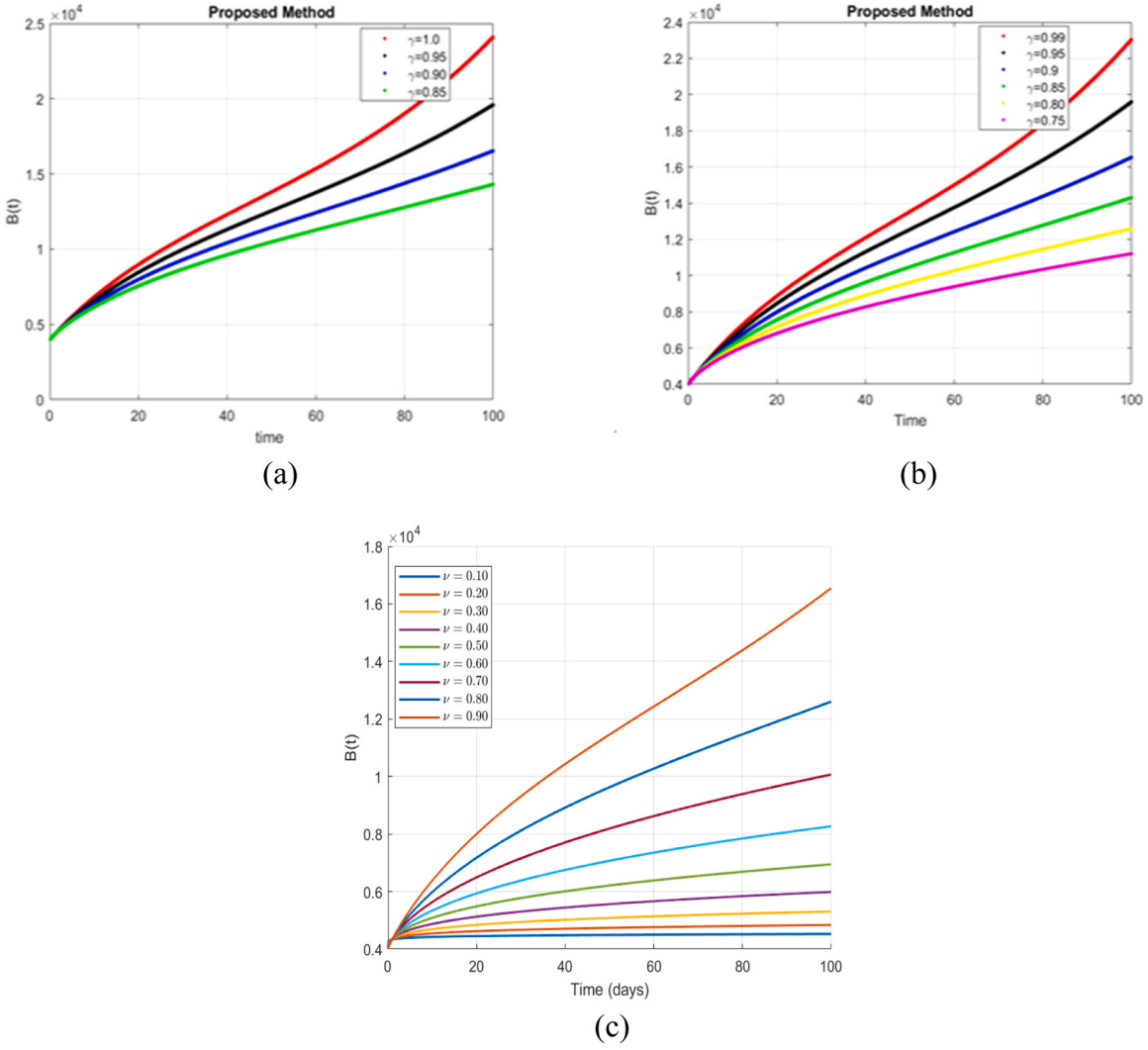

Fig. 12. Simulation of B(t) at different fractional and integer orders.

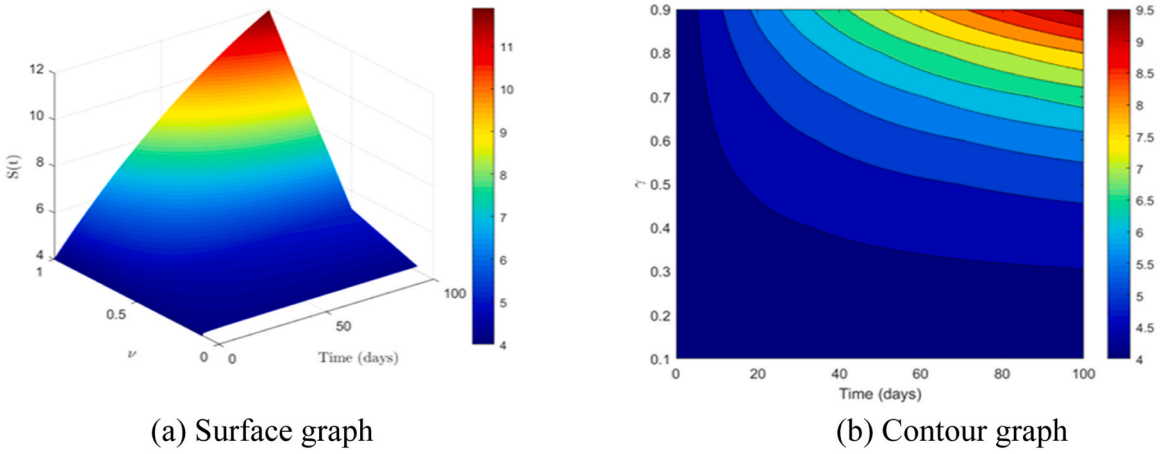

Fig. 13. Surface and contour graphs of S(t) at fractional values.

reproduction number is a crucial component in creating equilibrium. While the infection persists at an endemic level when $\mathbf{R_0} < \mathbf{1}$, it dies off when $\mathbf{R_0} > \mathbf{1}$. Unlike traditional models, the fractional-order framework demonstrated that transitions from disease-free to endemic states are slower and more influenced by previous system states, reflecting biological processes observed in the real world, such as environmental factors and persistent infection. A sensitivity study revealed that the infection rate and fractional parameter have a significant impact on the dynamics of illness, with larger memory effects leading to longer disease persistence and slower convergence to equilibrium. Our findings

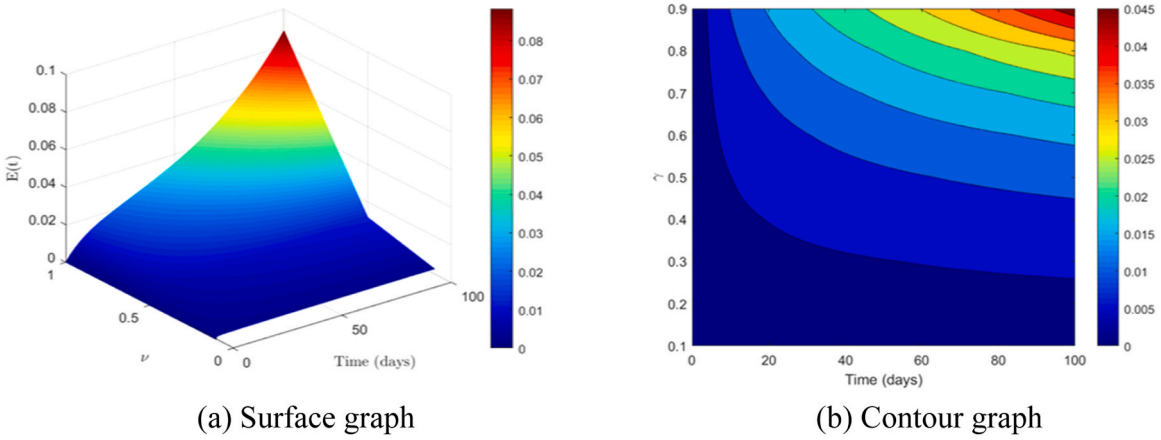

Fig. 14. Surface and contour graphs of E(t) at fractional values.

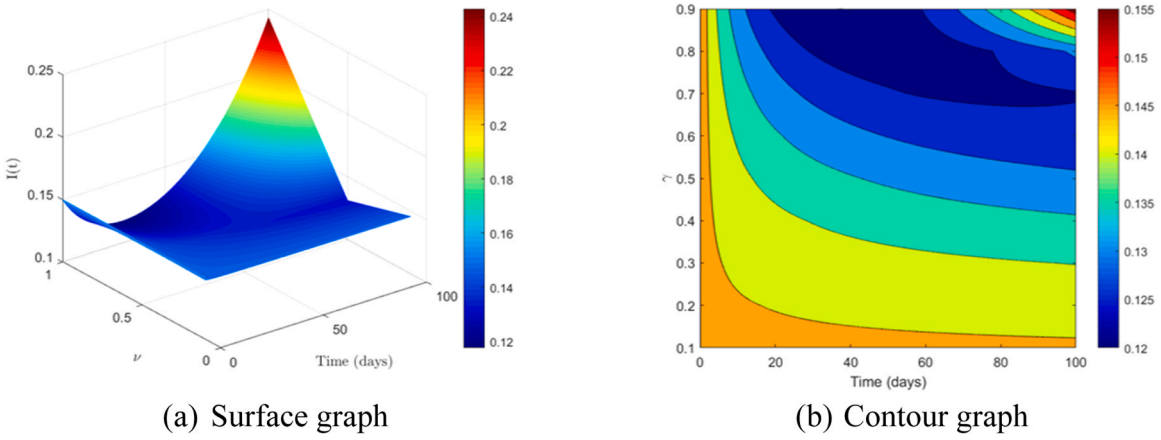

Fig. 15. Surface and contour graphs of I(t) at fractional values.

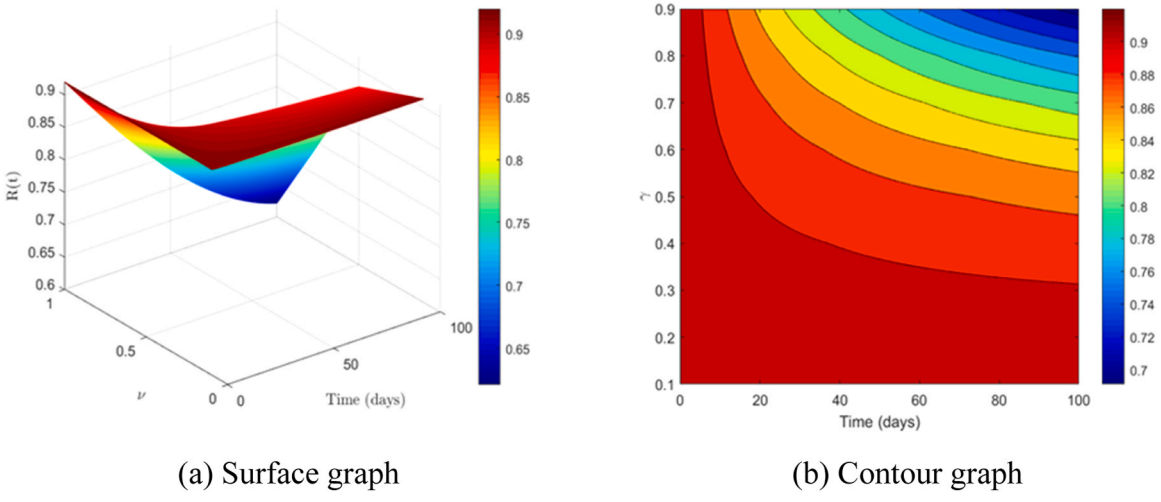

Fig. 16. Surface and contour graphs of R(t) at fractional values.

emphasize the importance of timely and consistent intervention strategies in disease management, as fractional models account for the delayed effects of both infection and control measures. Despite its theoretical nature, the study lays the groundwork for future research that combines field validation with empirical data, which could lead to the development of predictive tools for plant infection management. Finally, the use of fractional operators opens up new possibilities for developing more adaptable and effective control strategies for agricultural systems, as well as improving our mathematical understanding of how plant disease spreads. Extension workers can use this fractional-order FLS model in conjunction with real-time field data such as weather and crop health to generate actionable disease risk alerts, track disease progression, and guide management decisions via a user-friendly interface such as a mobile app or dashboard. Future directions include

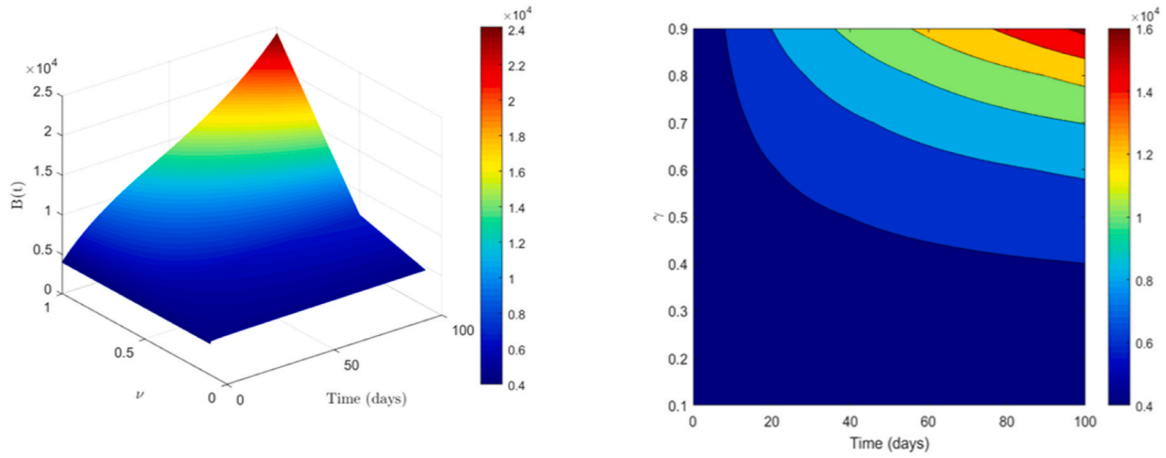

(a) Surface graph (b) Contour graph

Fig. 17. Surface and contour graphs of B(t) at fractional values.

improving model accuracy by integrating sensor data (e.g., drones, soil sensors), creating machine learning (ML) and deep learning (DL) algorithms to predict disease severity and optimize treatment, and broadening the model's scope to include various environmental factors and soybean varieties.

Author Statement

All the authors contributed equally to the writing of this paper. They read and approved the final version of the manuscript. Further all authors confirm that this work is original and has not been published elsewhere nor it is currently under consideration in whole or part for publication.

CRediT authorship contribution statement

Muhammad Farman: Writing - review & editing, Writing - original draft, Software, Methodology. **Izhar Ullah:** Conceptualization, Methodology, Investigation, Writing - Original Draft. **Evren Hincal:** Conceptualization, Methodology, Writing - Original Draft, Writing - Review and Editing, Software. **Kottakkaran Sooppy Nisar:** Conceptualization, Investigation, Writing - Review and Editing, Visualization. Visualization and Numerical Analysis. **Kamyar Hosseini:** Methodology, Investigation, Writing - Review and Editing, Formal Analysis, Software. **Aceng Sambas:** Conceptualization, Investigation, Writing - Original Draft, Writing - Review and Editing, Visualization.

Declaration of Competing Interest

I declare that we have no competing interest in publishing this article on behalf of all the authors.

Acknowledgements

This study is supported via funding from Prince Sattam bin Abdulaziz University project number (PSAU/2025/R/1446).

References

Abdullah, T.Q., Huang, G., Al-Sadi, W., Aboelmagd, Y., Mobarak, W., 2024. Fractional dynamics of cassava mosaic disease model with recovery rate using new proposed numerical scheme. Mathematics 12 (15), 2386.
Ackora-Prah, J., Seidu, B., Okyere, E., Asamoah, J.K., 2023. Fractal-fractional caputo maize streak virus disease model. Fractal Fract. 7 (2), 189.
Agrawal, V., Zhang, C., Shapiro, A.D., Dhurjati, P.S., 2004. A dynamic mathematical model to clarify signaling circuitry underlying programmed cell death control in Arabidopsis disease resistance. Biotechnol. Prog. 20 (2), 426–442.
Ahmad, A., Farman, M., Naik, P.A., Faiz, K., Ghaffar, A., Hincal, E., Saleem, M.U., 2024. Analytical analysis and bifurcation of pine wilt dynamical transmission with host vector and nonlinear incidence using sustainable fractional approach. Partial Differ. Equ. Appl. Math. 11, 100830.
Ahmad, A., Faiz, K., Farman, M., Sattar, S., Sambas, A., 2025. Control and effect of climate change due to human activities by a mathematical modeling approach under fractional operator. Model. Earth Syst. Environ. 11 (4), 1–21.
Akem, C.N., Dashiell, K.E., 1994. Effect of planting date on severity of frogeye leaf spot and grain yield of soybeans. Crop Prot. 13 (8), 607–610.
Ali, H.M., Ameen, I.G., Gaber, Y.A., 2024. The effect of curative and preventive optimal control measures on a fractional order plant disease model. Math. Comput. Simul. 220, 496–515.
Amelia, R., Anggriani, N., Istifadah, N., Supriatna, A.K., 2021. Stability analysis for the yellow virus disease mathematical model of red chili plants. Journal of Physics: Conference Series 1722 (1).
Athow, K., Probst, A.H., 1952. Phytopathology 42, 660–662.
Blyuss, K.B., Al Basir, F., Tsygankova, V.A., Biliavska, L.O., Iutynska, G.O., Kyrychko, S. N., Izhboldin, O.O., 2020. Control of mosaic disease using microbial biostimulants: insights from mathematical modelling. Ric. di Mat. 69, 437–455.
El Jarroudi, M., Karjoun, H., Kouadio, L., El Jarroudi, M., 2020. Mathematical modelling of non-local spore dispersion of wind-borne pathogens causing fungal diseases. Appl. Math. Comput. 376, 125107.
El-Sayed, A.M.A., Rida, S.Z., Gaber, Y.A., 2020. Dynamical of curative and preventive treatments in a two-stage plant disease model of fractional order. Chaos Solitons Fractals 137, 109879.
Farman, M., Shehzad, A., Akgül, A., Baleanu, D., Attia, N., Hassan, A.M., 2023. Analysis of a fractional order bovine brucellosis disease model with discrete generalized Mittag–Leffler kernels. Results Phys. 52, 106887.
Farman, M., Nisar, K.S., Shehzad, A., Baleanu, D., Amjad, A., Sultan, F., 2024. Computational analysis and chaos control of the fractional order syphilis disease model through modeling. Ain Shams Eng. J. 15 (6), 102743.
Farman, M., Nisar, K.S., Ali, M., Ahmad, H., Tabassum, M.F., Ghaffari, A.S., 2025. Chaos and forecasting financial risk dynamics with different stochastic economic factors by using a fractional operator. Model. Earth Syst. Environ. 11 (2), 146.
Farman, M., Sarwar, R., Hincal, E., Baleanu, D., Nisar, K.S., Sambas, A., Akram, M.M., 2025. Dynamical evaluation of the Mittag-Leffler properties-based marine ecosystem model. Earth Syst. Environ. 1–19.
Jiang, C., Wang, Y., Sun, Z., Chen, Z., 2025. Fractional-order equivalent circuit model for commercial sodium-ion batteries in a wide temperature range considering aging. J. Energy Storage 105, 114552.
Kumar, P., Baleanu, D., Erturk, V.S., Inc, M., Govindaraj, V., 2022. A delayed plant disease model with caputo fractional derivatives. Adv. Contin. Discret. Models 2022 (1), 11.
Li, C., Qian, D., Chen, Y., 2011. On Riemann-Liouville and caputo derivatives. Discret. Dyn. Nat. Soc. 2011 (1), 562494.
Manickam, A., Kavitha, M., Jaison, A.B., Singh, A.K., 2024. A fractional-order mathematical model of banana Xanthomonas wilt disease using caputo derivatives. Contemp. Math. 136–156.
McDonald, S.C., Buck, J., Li, Z., 2022. Automated, image-based disease measurement for phenotyping resistance to soybean frogeye leaf spot. Plant Methods 18 (1), 103.
Murwayi, A., Onyango, T., Owour, B., 2017. Mathematical analysis of plant disease dispersion model that incorporates wind strength and insect vector at equilibrium. Br. J. Math. Comput. Sci. 22 (5), 1–17.
Narayanan, G., Ahn, S., Wang, Y., Jeong, J.H., Joo, Y.H., 2025. Adaptive event-triggered stochastic estimator-based sampled-data fuzzy control for fractional-order

permanent magnet synchronous generator-based wind energy systems. Expert Syst. Appl. 261, 125536.
Nisar, K.S., Farman, M., Abdel-Aty, M., Ravichandran, C., 2024. A review of fractional order epidemic models for life sciences problems: past, present, and future. Alex. Eng. J. 95, 283–305.
Nisar, K.S., Farman, M., Abdel-Aty, M., Ravichandran, C., 2024. A review of fractional-order models for plant epidemiology. Prog. Fract. Differ. Appl. 10 (3), 489–521.
Phillips, X.A., Kandel, Y.R., Mueller, D.S., 2021. Impact of foliar fungicides on frogeye leaf spot severity, radiation use efficiency and yield of soybean in Iowa. Agronomy 11 (9), 1785.
Sharma, M., Kumar, C.J., Deka, A., 2022. Early diagnosis of rice plant disease using machine learning techniques. Arch. Phytopathol. Plant Prot. 55 (3), 259–283.
Ullah, M.A., Raza, N., Naik, P.A., Farman, M., Chahlaoui, Y., Huang, Z., 2025. Mathematical modeling and dynamical observations of HIV/AIDS transmission under the role of antiretroviral treatment. Comput. Methods Biomech. Biomed. Eng. 1–15.
Van den Driessche, P., 2017. Reproduction numbers of infectious disease models. Infect. Dis. Model. 2 (3), 288–303.
Vyska, M., Cunniffe, N., Gilligan, C., 2016. Trade-off between disease resistance and crop yield: a landscape-scale mathematical modelling perspective. J. R. Soc. Interface 13 (123), 20160451.
Xu, C., Farman, M., Shehzad, A., Sooppy Nisar, K., 2025. Modeling and Ulam–Hyers stability analysis of oleic acid epoxidation by using a fractional-order kinetic model. Math. Methods Appl. Sci. 48 (3), 3726–3747.
Yang, C., Wang, J., 2023. A mathematical model for frogeye leaf spot epidemics in soybean. Math. Biosci. Eng. 21 (1).
Zhao, T., Xiao, Y., 2015. Plant disease models with nonlinear impulsive cultural control strategies for vegetatively propagated plants. Math. Comput. Simul. 107, 61–91.